MODELING CREEP INA ROTATING COMPOSITE DISC OF VARIABLE THICKNESS

A Thesis report submitted
in partial fulfilment of the requirements for
the award of degree of

MASTER OF ENGINEERING
IN
CAD/CAM & ROBOTICS

Submitted by

HEMANT KUMAR KAUSHIK

ROLL NO.8048108

Under the Guidance of

Dr.V.K.GUPTA
Reader, M.E.D.
Univ.College of Engineering
Punjabi University,Patiala

Mr. TARUN NANDA
Lecturer, M.E.D.
T.I.E.T, Patiala

MECHANICAL ENGINEERING DEPARTMENT
THAPAR INSTITUTE OF ENGINEERING AND TECHNOLOGY
(DEEMED UNIVERSITY) PATIALA-147004, PUNJAB

June, 2006

CERTIFICATE

This is to certify that the thesis titled, **"MODELING CREEP IN A ROTATING COMPOSITE DISC OF VARIABLE THICKNESS**", being submitted by **Mr. HEMANT KUMAR KAUSHIK**, in partial fulfillment of the requirement for the award of degree of **MASTER OF ENGINEERING (CAD/CAM & ROBOTICS)** at **Mechanical Engineering Department**, **Thapar Institute of Engineering and Technology (Deemed University), Patiala,** is a bonafide work carried out by him under our guidance and supervision and that no part of this seminar has been submitted for the award of any other degree.

Dr. V. K. GUPTA
Reader,
Deptt. of Mechanical Engineering,
Univ. College of Engg.,
Punjabi University, Patiala-147004.

Mr. TARUN NANDA
Lecturer,
Deptt. of Mechanical Engineering,
T. I. E. T, Patiala-147004.

(Dr. S.K. Mohapatra)
Professor& Head, M.E.D.,
Thapar Inst.of Engg. &Tech.
Patiala-147004 (Punjab)

(Dr. T.P.Singh)
Dean Academic Affairs
Thapar Inst. of Engg. & Tech.
Patiala-147004 (Punjab)

ACKNOWLEDGEMENT

I express my sincere gratitude to my guides, **Dr V.K.Gupta**, Reader, **Mechanical Engineering Department, Univ.College of Engg, Punjabi University** and **Mr. Tarun Nanda,** Lecturer, **Mechanical Engineering Department, Thapar Institute of Engineering & Technology,** for their valuable guidance, proper advice and constant encouragement during the course of my work on this thesis. Without their help this report wouldn't have seen the light of the day.

I am also grateful to our PG-Coordinator **Dr. Vijay Kumar Jadon** for successfully carrying the framework for the thesis.

I am also thankful to all my friends, who devoted their valuable time and helped me in all possible ways towards successful completion of my thesis work

I do not find enough words with which I can express my feeling of thanks to entire faculty and staff of **Mechanical Engineering Department, Thapar Institute of Engineering & Technology,** for their help, inspiration and moral support, which went a long way in successful completion of my thesis.

I would like to thank **all my friends** again for making my stay at T.I.E.T., Patiala very enjoyable and memorable. I will cherish the moments forever.

(HEMANT KUMAR KAUSHIK)

Roll No. 8048108

ABSTRACT

Rotating discs made of discontinuously reinforced aluminium matrix composite (DRAMC) are widely used in gas turbines, jet engines, automotive and aerospace braking systems, and are usually operated at relatively higher angular speed and subjected to high temperature/ thermal gradient. Therefore, the prediction of long-term steady state creep deformations is very important for these applications.

The steady state creep behavior of a rotating disc having variable profile has been modeled in this thesis. The material of the disc is assumed to be 6061Al-$SiC_{P,W}$ and undergo steady state creep described by Sherby's law. The creep behavior of disc having (i) linearly varying thickness, (ii) hyperbolically varying thickness have been obtained and compared with those obtained for disc having uniform thickness. The volume of all the discs is kept the same. The study revealed that the stress and the strain rates in the disc can be reduced to a great extent by varying the disc profile. The effect of disc profile on the creep behavior is much prominent in anisotropic disc compared to isotropic disc.

TABLE OF CONTENTS

CONTENTS	PAGE NO.
CERTIFICATE	iii
ACKNOWLEDGEMENT	iv
ABSTRACT	v
TABLE OF CONTENTS	**vi**
LIST OF FIGURES	viii
CHAPTER 1: INTRODUCTION	1
1.1 History of Composites	1
1.2 Mechanical advantage of Composite Materials	2
1.2.1 Material Selection Parameters	3
1.3 Classification of Composite Materials	3
1.3.1 Classification based on Geometry of Reinforcement	4
a) Particulate Composite	4
b) Flake Composite	4
c) Fiber Composite	4
1.3.2 Classification based on Matrix	5
a) Polymer Matrix composite	5
b) Metal Matrix Composite	5
c) Ceramic Matrix Composite	6
d) Carbon –Carbon Composite	6
1.4 Aluminium/Aluminium alloy based MMCs	6
1.4.1 Properties of Aluminium based MMCs	7
a) Specific Stiffness	7
b) Specific strength	7
c) Fatigue Resistance	7
d) Coefficient of Thermal Expansion	7
e) Wear Resistance	8
1.5 Typical Applications of Aluminium Matrix Composites	8
1.6 Functionally Gradient Materials (FGMs)	11

CHAPTER 2: LITERATURE REVIEW 13
2.1 Creep
2.2 Yield Criteria for Ductile Materials 15
2.2.1 Distortion Energy Criterion (VON Mises Criterion) 15
2.2.2 Maximum Shear-Stress Criterion (Tresca Yield Criterion) 16
2.2.3 Hill Anisotropy Criteria 17
2.2.4 Hoffman Yield Criterion 19
2.3 Creep Laws 20
2.4 Constitutive Equation for Creep under Multiaxial Loading 21
2.5 Rotating Disc and Creep 22
CHAPTER 3: PROBLEM FORMULATION 28
CHAPTER 4: MATHEMATICAL ANALYSIS OF CREEP 29
4.1 Assumptions 29
4.2 Analysis of Creep 30
4.3 Equilibrium Equation for Rotating Disc 34
4.4 Disc Profiles 36
4.5 Calculation of Area and Inertia of Discs 38
4.6 Creep Parameters 38
4.7 Anisotropic Constants 39
4.8 Solution Procedure 41
CHAPTER 5: RESULTS AND DISCUSSIONS 42
5.1 Effect of Disc Profile on Isotropic Disc 42
5.2. Effect of Disc Profile on Anisotropic Disc 43
CHAPTER 6: CONCLUSION 49
FUTURE SCOPE OF WORK 50
REFERENCES 51

LIST OF FIGURES

Fig. No.	*Title*	*Page No.*
Fig.1.1:	Thin Slabs in Plywood	2
Fig 1.2:	Classification of Composite materials	3
Fig 1.3:	Particles as the reinforcement (Particulate composites)	4
Fig 1.4:	Flat flakes as the reinforcement (Flake composites)	4
Fig 1.5:	Random fiber (short fiber) reinforced composite	5
Fig 1.6:	Continuous fiber (long fiber) reinforced composites	5
Fig1.7:	Morphology of Reinforcement in Matrix	5
Fig1.8:	Use of Composite Materials in Air Craft	9
Fig 1.9:	Application of composites in various sectors [2]	10
Fig1.10:	Characteristics of FGMs [5]	11
Fig.2.1:	Creep curve showing the three stages of creep	14
Fig.2.2:	Comparison of Von Mises and Tresca Criterion	17
Fig 2.3:	Yield locus for textured titanium-alloy sheet	19
Fig 4.1:	Free body diagram of an element of the disc	34
Fig.4.2.	Variation of disc thickness with radial distance for different discs	37
Fig 5.1:	Tangential stress versus radius for discs of the same volume but different profile (Isotropic)	45
Fig 5.2:	Radial stress versus radius for discs of the same volume but different profile (Isotropic)	45
Fig 5.3:	Tangential strain rate versus radius for discs of the same volume but different profile (Isotropic)	46

Fig 5.4: Radial strain rate versus radius for discs of the same volume but different profile (Isotropic) 46

Fig 5.5: Tangential stress versus radius for discs of the same volume but different profile (Anisotropic) 47

Fig 5.6: Radial stress versus radius for discs of the same volume but different profile (Anisotropic) 47

Fig 5.7: Tangential strain rate versus radius for discs of the same volume but different profile (Anisotropic) 48

Fig 5.8: Radial strain rate versus radius for discs of the same volume but different profile (Isotropic) 48

CHAPTER 1

INTRODUCTION

In the continuing quest for improved performance , which may be specified by various criteria including weight reduction, more strength and lower cost, currently used engineering materials have reached the limit of their usefulness. Thus materials scientists are always striving to produce either improved traditional materials or completely new materials. Composite materials are an example of the later type.

A composite material is combination of two or more macro constituents differing in the form and/or composition that are essentially insoluble in each other. The composite materials possess characteristic properties, such as high stiffness and strength, low weight, high temperature performance, good corrosion resistance, high hardness and conductivity that are not possible in any of its constituents alone. Analysis of these properties reveals that they depend on the following:

- Properties of the individual constituents.
- Relative amounts of the constituents.
- Size and shape of the constituents (i.e. Morphology).
- Degree of bonding between constituents.
- Orientation of the various constituents.

1.1 History of Composites

One of the earliest known composite materials is adobe brick in which straw (a fibrous material) is mixed with mud or clay (an adhesive with strong compressive strength). The straw allows the water in the clay to evaporate and distribute cracks in the clay uniformly, greatly improving the strength of this early building material. Another form of a composite material is the ubiquitous construction material called plywood. Plywood (Fig.1.1) uses natural materials (thin slabs of wood) held together by a strong adhesive, making the structure stronger than just the wood itself. In nature, bamboo is often cited as an example of a wood composite structure, combining a cellulose fiber and lignin, with the

lignin providing the adhesive to hold the fibers together.

Fig.1.1: Thin Slabs in Plywood

Reinforced concrete is a combination of two remarkable materials, concrete (a composite by itself) and steel that takes advantage of the strengths of each material to overcome their individual limitations in each. Steel has very high tensile strength, while concrete has very high compressive strength. In combination, they make a superior material for road and bridge construction.

Today, when we speak of composite materials, or just 'composites', we are referring to the highly engineered combinations of polymer resins and reinforcing materials such as glass fibers. A fiberglass composite structure is a combination of glass fibers of various lengths and resins such as vinyl ester or polyester. The term FRP is often used, meaning Fiber Reinforced Plastic. FRP is a very general term for many different combinations of reinforcement materials and bonding resins. Thus, the term "composites" is used extremely broadly to describe many materials with many different properties targeted at an even larger number of applications. To show how composites have changed our world, look no further than under the hood of a modern car and realize that most of what we can see are components made of composite materials [1].

1.2 Mechanical advantage of Composite Materials

Following two parameters are commonly used to measure the relative advantage derived from composite materials.

(a). Specific modulus

(b). Specific strength

Specific modulus is defined as the ratio of Young's Modulus (E) and density (ρ) of the materials.

Specific strength is defined as ratio between strength and density of the materials.

These two ratios are high in composite materials. As an example the strength of a graphite/epoxy unidirectional composite material is same as steel but the specific strength of composite material is three times that of steel. This means that for the same application of a rod, we required $1/3^{rd}$ diameter than that of steel, thereby saving material and energy costs.

1.2.1 Material Selection Parameters

For selecting a composite material for a particular application, the following six parameters are to be considered:

(i) Strength

(ii) Toughness

(iii) Formadibility

(iv) Joinability

(v) Corrosion

(vi) Wear Resistance

(vii) Affordability.

1.3 Classification of Composite Materials

Composites are classified [2] by the geometry of the reinforcement as particulate, flake and fiber or by the type of matrix as polymer, metal, ceramic and carbon as shown in Fig.1.2.

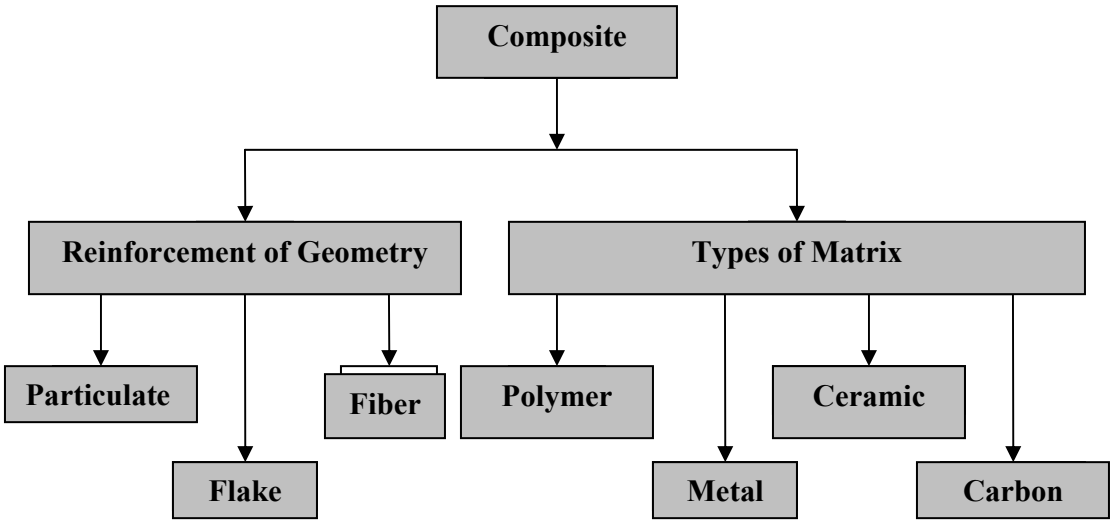

Fig 1.2: Classification of Composite materials

1.3.1 Classification based on Geometry of Reinforcement

Based on this, the composites are of the following types [2]:

(a) Particulate Composites

(b) Flake Composites

(c) Fiber Composites

(a) **Particulate Composites**

This class of composite consists of particles reinforced in a matrix of metal, alloy or ceramics shown in Fig.1.3. They usually exhibit isotropic properties. Particulate composites have advantages such as improved strength, increased operating temperature and oxidation resistance.

(b) **Flake Composites**

It consists of flat reinforcement in the matrix as shown in Fig.1.4. Typical flake materials are glass, mica, aluminum and silver. Flake composites provide advantages such as high out of plane flexural modulus, higher strength and low cost. However, flakes can not be oriented easily; therefore a limited number of materials are available for use.

(c) **Fiber Composites**

These composites consist of matrix reinforced by short (discontinuous) or long (continuous) fiber. Fibers are generally anisotropic and examples include carbon aramids Fig.1.5.

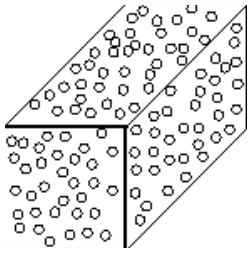

Fig (1.3) Particles as the reinforcement (Particulate composites)

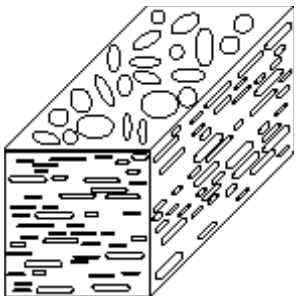

Fig (1.4) Flat flakes as the reinforcement (Flake composites)

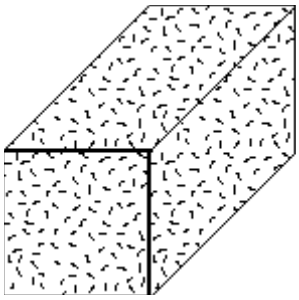

Fig.(1.5) Random fiber (short fiber) reinforced composite

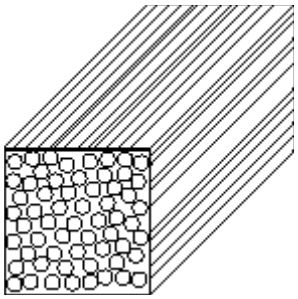

Fig (1.6) Continuous fiber (long fiber) reinforced composites

Fig1.7: Morphology of Reinforcement in Matrix

1.3.2 **Classification based on Matrix**

Based on the type of matrix, Composites are of the following types [2]:

(a) Polymer Matrix Composite (PMC)

(b) Metal Matrix Composite (MMC)

(c) Ceramic Matrix Composite (CMC)

(d) Carbon –Carbon Composite

(a) Polymer Matrix Composite (PMC)

Polymer matrix composites are the most advanced composites. These composites consist of a polymer (e.g., epoxy, polyester, urethane etc) reinforced by thin-diameter fibers(e.g., graphite , aramids, boron etc).These are commonly employed due to their low cost, high strength, and simple manufacturing principle. As an example, graphite/ epoxy composites are approximately five times stronger than steel on a weight-for-weight basis. Main drawback of Polymer Matrix Composites (PMCs) include low operating temperature, high coefficient of thermal and moisture expansion and low elastic properties in certain directions. However, the advantages include its strength, low cost, high chemical resistance and good insulating property.

(b) Metal Matrix Composite (MMC)

This class of composite materials consists of metallic matrix which is usually ductile. The ductile matrix can be aluminum, copper, magnesium, titanium, nickel, super alloy or even an intermetallic compound. The reinforcing fibers may be graphite, boron carbide, alumina or silicon carbide. Fine whiskers of sapphire, silicon carbide, silicon nitride, wires of titanium, tungsten, molybdenum, beryllium and stainless steel etc have also been used as reinforcement.

Compared to conventional engineering materials, these composites offer higher stiffness and strength, especially at elevated temperatures, low coefficient of thermal expansion and enhanced resistance to fatigue, abrasion and wear. Compared to organic matrix materials, they offer high heat resistance and improved electrical and thermal conductivity.

Graphite-reinforced aluminum can be designed to have near zero thermal expansion in the fiber direction. Aluminum oxide-reinforced aluminum matrix composites have been extensively used in automotive connecting rods to provide high stiffness with low weight. Aluminum reinforced with silicon carbide whiskers has been fabricated into aircraft wing panels , providing 20-40% weight saving .Fiber reinforced super alloy has potential future for applications such as turbine blades.

(c) Ceramic Matrix Composite (CMC)

Ceramic matrix composites possess properties like high melting points, good corrosion resistance, stability at elevated temperatures and high compressive strength.

These materials can even be used at very high temperatures (i.e. above 1500°C).

(d) Carbon –Carbon Composite

These composites retain their properties even at exceptionally very high temperatures in the range of 3315°C. Their dimensional stability is also good and therefore can be used at elevated temperatures. They are 20 times stronger and 30% lighter than the Graphite fibers.

Carbon by itself is brittle and flaw sensitive like the ceramics. Reinforcement of the carbon matrix allows the composite to fail gradually and also gives advantages such as ability to withstand high temperatures, low creep at high temperatures, low density, good tensile and compressive strengths, high fatigue resistance, high thermal conductivity and high coefficient of friction.

1.4 **Aluminum /Aluminum alloy based MMCs**

In research and development as well as in various industrial applications, MMCs based on aluminum and their alloys are widely used [3].This is because aluminum is light in weight which is the primary requirement in most of the applications of the metal matrix composites. Additionally, it is economical in comparison with other light metals, such as titanium and magnesium. Further its excellent strength, ductility and corrosion properties are well established and they can be modified to fulfil the requirements of various applications ranging from automotive and aircraft industry to sports and leisure. The development work of aluminum matrix composite is currently concentrated on two sectors:

(i) Continuous fiber reinforced composite with superior properties for every specific applications.

(ii) Mass production technologies of inexpensive discontinuously reinforced composites with moderate properties for wider range of applications.

Metal matrix composites possess set of properties that are of interest to the designers for application of both, structural and non-structural nature.

1.4.1 **Properties of Aluminum based MMCs**

The salient properties of aluminum based MMCs are discussed below [3]:

(a) Specific Stiffness

The addition of stiff metallic or ceramic reinforcement materials to the metal matrix results in an increase in elastic modulus of the composites materials. In case of light weight

metals, such as aluminum, titanium and magnesium, the increase can be very significant even at moderate levels of reinforcement addition. Typical ceramic reinforcements are similar in density to the light weight metal matrices, and one of the primary benefits of these is their increased specific stiffness.

(b) Specific Strength

In addition to high stiffness, aluminum based MMCs also possess high strength. The strength of the composite is strongly dependent on the specific characteristics of the reinforcement material, their morphology, and the type of bonding with the metal matrix. Continuous fiber reinforced composites exhibit high specific strength levels in the direction of the fiber orientation. Particulate reinforced MMCs exhibit specific strength ranging up to double over the metal matrix depending on the matrix alloy as well as reinforcement type and their volume fraction.

(c) Fatigue Resistance

The addition of reinforcement in aluminium/aluminium alloy matrix significantly improves the fatigue resistance. The mechanisms of fatigue resistance enhancement differ in composites depending on the morphology of the reinforcement and characteristics of reinforcement-matrix interface.

(d) Coefficient of Thermal Expansion

The typical ceramic reinforcements for MMCs have significantly lower values of the coefficient of thermal expansion than the metal matrix into which they are incorporated. Thus, the addition of ceramic reinforcement to the high expansion metals such as aluminum, magnesium, copper, and titanium can result in substantial reduction in the coefficient of thermal expansion.

(e) Wear Resistance

The increased hardness of the typical, ceramic reinforcement materials can also affect the tribological properties of the metal matrix composites relative to the unreinforced matrix. However the MMCs based on light metals (aluminum, magnesium and titanium), due to lack of wear resistance have limited applications in areas where weight saving could be potentially obtained. Particle reinforced MMCs have been of particular interest for use in wear resistance dominated applications.

1.5 Typical Applications of Aluminum Matrix Composites

This section discusses some typical applications of discontinuously reinforced aluminum matrix composite (DRAMC) [4]:

(i) Aircraft

A significant portion of aircraft structure is designed by stiffness, as a result many of the aircraft structural applications for MMCs seek to capitalize on the increased specific stiffness that aluminum based MMCs provide. Aircraft structural applications actually require a combination of properties including adequate strength, damage tolerance and corrosion resistance. MMCs have lower damage tolerance properties than their unreinforced metal matrix counterparts. Silicon carbide particle reinforced aluminum MMC have been used in the US AIR Force F-16 Aircraft (Fig.1.8).

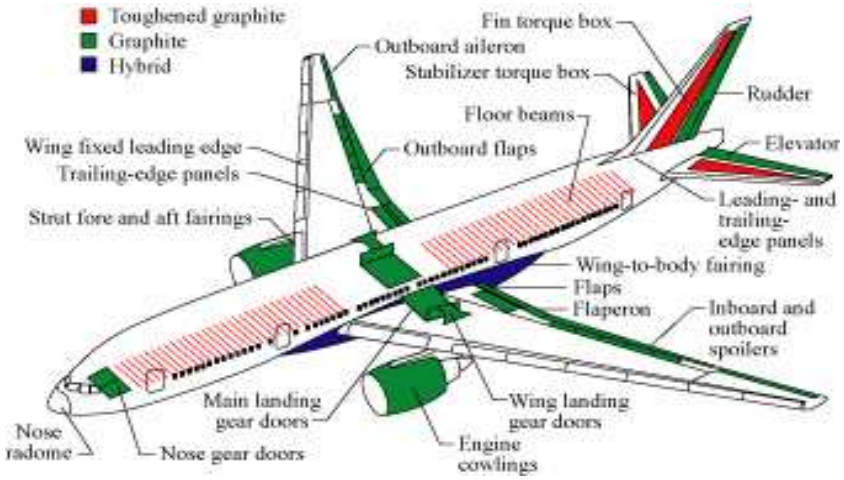

Fig1.8: Use of Composite Materials in Air Craft

(ii) Aero-Engine

Aluminum based MMCs have been used in aero engines, especially in the area of fan exit guide vanes. In this application, both specific stiffness and specific strength, especially at elevated temperature, are the critical properties. Similar to aircraft structure, other properties, including fatigue, creep and oxidation resistance are also very important in these applications.

(iii) Brake System

Aluminum based MMCs offer a very useful combination of properties for brake

system application in replacement of cast iron. Specially, the wear resistance and high thermal conductivity of aluminum based MMCs enable substitution of cast iron in disk brake rotors and brake drums with an attendant weight saving of the order of 50-60%. This helps in reducing inertia force and provides additional benefits. The light weight MMCs rotor also provides increased acceleration and reduced braking distance.

(iv) Other Automotive Applications

MMCs, especially those based on Aluminum matrices, are candidates for application in automotive sector. Typical automotive applications are listed in Table1.1 [4]. Fig 1.9 depicts the applications of composite materials in various sectors.

Table No.1.1 Typical Automotive Applications of Al/Al based MMCs [4]

Products	MMCs System	Characteristics of applied MMCs	Year(Maker)
Vane, Pressure side plate of oil pressure vane pump	Al_2O_3- SiO_2	Wear Resistance	1987(Hiroshima Aluminum)
Ring, Groove Reinforced Piston	Al_2O_3/Al-alloy	Light weight, Wear resistance at elevated temperature	1983 (Toyota)
Shock absorber	SiC_P/Al-alloy	Light weight ,Wear resistance, Thermal diffusivity	1989 (Mitsubishi Aluminum)
Bicycle frame	SiC_W/6061	Light weight ,High specific rigidity	1989 (Kobe steel)
Diesel engine piston	SiC_W/Al-alloy	Light weight ,Wear Resistance	1989 (Niigata)

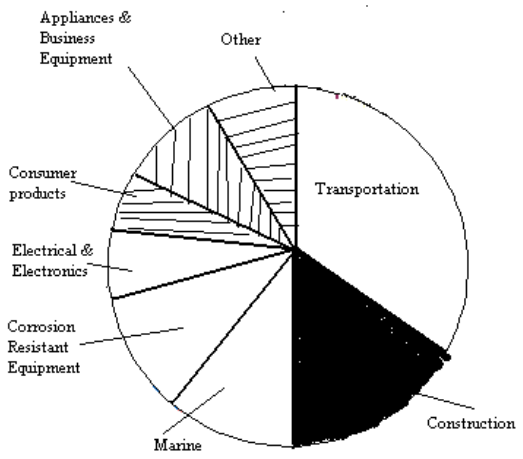

Fig 1.9: Application of composites in various sectors [2]

1.6 Functionally Gradient Materials (FGMs)

In 1987, a national project was initiated in Japan [5] under the title 'Research on the Basic Technology for the Development of Functionally Gradient Materials for Relaxation of Thermal-Stress'. The project was aimed to develop advanced heat shielding structural materials for future space programs.

In general, the highest temperature on the surface of space –plane is estimated on reach 2100K. Therefore material at the surface must be able to temperature as high as 2100K and temperature difference of 1600K. Currently, no industrial material is known that can withstand such severe thermo-mechanical loading. The concept of FGM has been proposed to prepare a new composite by using heat resistant ceramic on the high-temperature side and tough metals with high thermal conductivity on the low-temperature side, with a gradual compositional variation from ceramic to metal. FGMs are therefore composite materials with a macroscopically inhomogeneous character. Continuous changes in composition result in gradient in the properties of FGMs. The difference in microstructure and properties between FGMs and conventional composite materials are illustrated in Fig.1.6.

Function/ Property	Mechanical Strength Thermal Conductivity	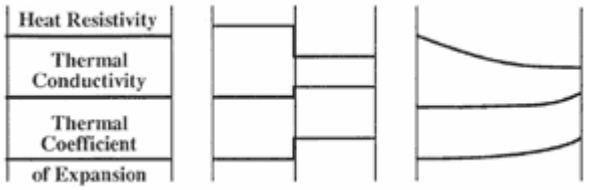
Structure/ Texture	Constituent Elements: Ceramic ∘ Metal •	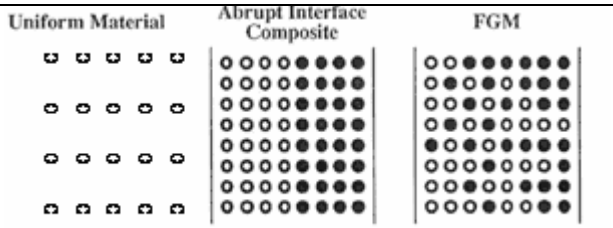
Materials	Example	Convent. Composites FGM

Fig1.10: Characteristics of FGMs [5]

FGMs offer great promise in applications where the operating conditions are severe.

FGMs are ideal candidates for applications involving severe thermal gradients, ranging from thermal structures in advanced aircraft and aerospace engines to computer circuit boards. Other examples are wear resistant linings for handling large and heavy abrasive particles, rocket heat shields, heat exchanger tubes, and thermoelectric generators, heat-engine components, plasma facing for fusion reactors and electrically insulating metal/ceramic joints. FGMs are also ideal for minimizing thermo-mechanical mismatch in metal-ceramic bonding.

CHAPTER 2

LITERATURE REVIEW

The application of composite materials in engineering, particularly in structural applications, is increasing in scope and several relatively new aspects of materials behavior are being addressed, for example, the long term behavior under mechanical, thermal and chemical/environmental loadings. The present study concerns the creep performance, which is of considerable interest. The experimental testing and evaluation of the many available composite material systems are very complex, costly as well as time consuming. Therefore, the prediction and analysis of creep properties for the assessment of service life of the components made of composite materials, is of great practical importance for practicing engineers.

2.1 Creep

The progressive deformation of a material at constant load is called creep. To determine the engineering creep curve of a metal, a constant load is applied to a tensile specimen maintained at a constant temperature and the strain (extension) is determined as a function of time.

Curve A in the Fig.2.1 illustrates the idealized shape of the creep curve. The slope of this curve ($d\varepsilon/dt$) is referred to as the creep rate. A typical creep curve exhibits three stages which are readily distinguishable and depend strongly on the applied stress and temperature.

The first stage of the creep, known as primary creep, represents a region of decreasing creep rate. Primary creep is a period of predominantly transient creep in which the resistance of the material increases by virtue of its own deformation. Primary creep occurs at low temperature and low stress levels.

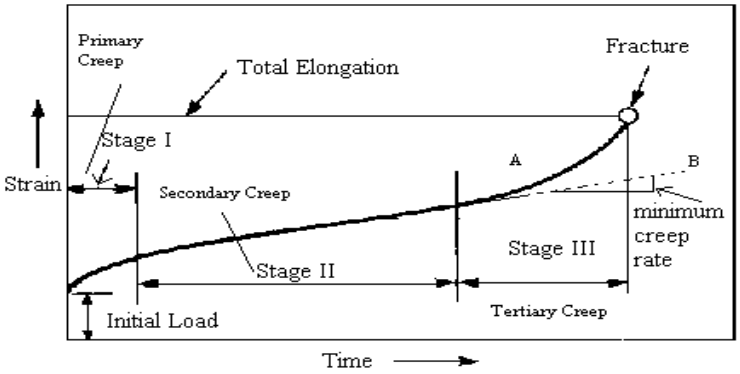

Fig.2.1 Creep curve showing the three stages of creep.
(Curve A- Constant load curve, Curve B- Constant stress test).

The second stage of creep, known also as secondary creep, is a period of nearly constant creep rate which result from a balance between the competing processes of strain hardening and recovery. For this reason, secondary creep is usually referred to as **Steady State Creep**. The average value of the creep rate during secondary creep is called the minimum creep rate.

Third stage or tertiary creep mainly occurs in constant load creep tests at high stresses and high temperature. Tertiary creep occurs when there is an effective reduction in cross-sectional area either because of necking or internal void formation. Third stage creep is often associated with metallurgical changes such as coarsening of precipitate particles, recrystallization or diffusional changes in the phases present.

The dashed line (Curve B) in Fig.2.1 shows the shape of a constant-stress creep curve. In engineering situations, it is usually the load, not the stress that is maintained constant, so a constant load creep test is more important [6].

Garofalo [6] has proposed that the creep curve can be represented by the following equation for a limited number of materials.

$$\varepsilon = \varepsilon_0 + \varepsilon_t(1 - e^{-rt}) + \varepsilon'$$

where, ε is total strain, ε_0 is the instantaneous strain on loading, ε_t is the limit for transient creep, r is the ratio of transient creep rate to the transient creep strain, and ε' is the steady

state creep rate.

2.2 Yield Criteria for Ductile Materials

Aluminum based MMCs are ductile in nature therefore, this section discusses the yield criteria applicable for ductile materials. The problem of deducing mathematical relationships for predicting the conditions at which plastic yielding begins when a material is subjected to any possible combination of stress is an important consideration in the field of plasticity. Under uniaxial loading, as in a tension test, macroscopic plastic flow begins at the yield stress σ_y. It is expected that yielding under a situation of combined stresses can be related to some particular combination of principal stresses.

2.2.1 Distortion Energy Criterion (Von Mises Criterion)

The criteria for predicting the onset of yielding in ductile metals is Von Mises or, Distortion-Energy Criterion [6].Von Mises has proposed that yielding would occur when the second invariant of the stress deviator J_2 exceeds some critical value;

$$J_2 = \frac{1}{6}\left[(\sigma_1-\sigma_2)^2+(\sigma_2-\sigma_3)^2+(\sigma_3-\sigma_1)^2\right] = k^2 \qquad (2.1)$$

To evaluate the constant k and relate it to yielding in the tension test, it is realized that at yielding in uniaxial tension $\sigma_1=\sigma_y$, $\sigma_2=\sigma_3=0$;

$$\sigma_y^2+\sigma_y^2=6k^2$$

$$\sigma_y=\sqrt{3}k \qquad (2.2)$$

Substituting Eq (2.2) in Eq. (2.1) results in the usual from of the Von Mises yield criterion

$$\sigma_y=\frac{1}{\sqrt{2}}\left[(\sigma_1-\sigma_2)^2+(\sigma_2-\sigma_3)^2+(\sigma_3-\sigma_1)^2\right]^{1/2} \qquad (2.3)$$

Therefore, yielding would occur when the differences of stresses on the right side of eq. (2.3) exceeds the yield stress in uniaxial tension σ_y. Since the Von Mises yield criterion

is based on differences of normal stresses, (σ_1-σ_2) etc, the criterion is independent of the component of hydrostatic stress. Further, the Von Mises yield criterion involves squared terms, the results is independent of the sign of the individual stresses. This is an important advantage since it is not necessary to know which are the largest and smallest principal stresses in order to use this yield criterion.

2.2.2 Maximum Shear Stress Criterion (Tresca Yield Criterion)

The criterion assumes that yielding occurs when the maximum shear stress reaches the value of the shear stress in the uniaxial tension test. The maximum shear stress [6] is given by,

$$\tau_{max} = \frac{\sigma_1 - \sigma_3}{2} \tag{2.4}$$

where, σ_1 is the algebraically largest and σ_3 is the algebraically smallest principal stress.

For uniaxial tension, $\sigma_1=\sigma_y$, $\sigma_2=\sigma_3=0$ and the shearing yield stress τ_y is equal to $\sigma_y/2$.

Therefore, Eq. (2.4) becomes,

$$\tau_{max} = \frac{\sigma_1 - \sigma_3}{2} = \tau_y = \frac{\sigma_y}{2} \tag{2.5}$$

Therefore, the maximum shear stress criterion is given by

$$\sigma_1-\sigma_3= \sigma_y \tag{2.6}$$

For a state of pure shear, $\sigma_1= -\sigma_3=k$, $\sigma_2=0$, the maximum shear stress criterion predicts that yielding will occur when,

$$\sigma_1-\sigma_3=2k=\sigma_y$$

This equation can be rewritten as, $k= \frac{\sigma_y}{2}$ (2.7)

Hence, the maximum shear stress criterion may be written as,

$$\sigma_1-\sigma_3=2k \tag{2.8}$$

The maximum shear stress criterion is mathematically less complicated than the Von Mises criterion [6], and for this reason it is often used in engineering design. Fig.2.2 shows graphical comparison of Von Mises and Tresca Yield criteria.

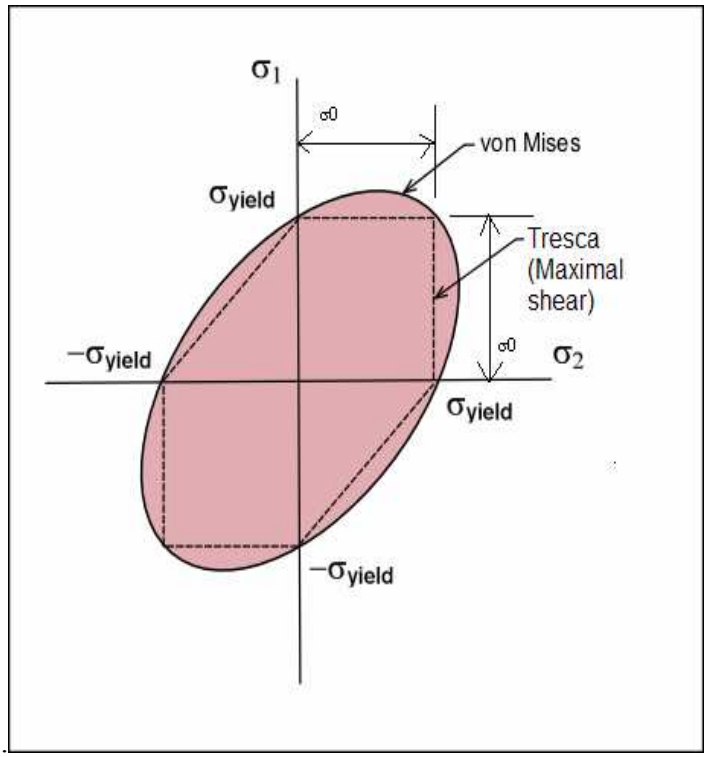

Fig.2.2. Comparison of Von Mises and Tresca Criterion

2.2.3 Hill Anisotropy Criterion

The yield criteria considered so far assumes that the material is isotropic. While this may be the case at the start of plastic deformation, it certainly is no longer a valid assumption after the metal has undergone appreciable plastic deformation. Moreover, most fabricated metal shapes have anisotropic properties, so that it is likely that the tubular specimens used for basic studies of yield criteria incorporate some degree of anisotropy. Certainly the Von Mises criterion as given by Eq (2.3) would not be valid for a highly oriented cold-rolled sheet or a fiber–reinforced composite material.

Hill [6] has formulated the Von Mises yield criterion for an anisotropic material having orthotropic symmetry as given below,

$$F(\sigma_y-\sigma_z)^2+G(\sigma_z-\sigma_x)^2+H(\sigma_x-\sigma_y)^2+2L\tau_{yz}^2+2M\tau_{zx}^2+2N\tau_{xy}^2=1$$

where, σ_x, σ_y and σ_z are normal stresses along x, y and z directions respectively. τ_{yz}, τ_{zx}, τ_{xy} are shear stresses and F, G, H, L, M and N are constants defining the degree of anisotropy. For principal axes of orthographic symmetry, the above equation reduces to following form,

$$F(\sigma_y-\sigma_z)^2+G(\sigma_z-\sigma_x)^2+H(\sigma_x-\sigma_y)^2=1 \qquad (2.9)$$

If x, y and z are the yield stresses in the principal direction 1, 2, 3 respectively, then by substituting in Eqn. (2.9), we can evaluate the constants as,

$$G+H=\frac{1}{x^2}$$

$$H+F=\frac{1}{y^2}$$

$$F+G=\frac{1}{z^2}$$

Lubahn and Felgar [6] have given detailed plasticity calculation for anisotropic behavior. On a plane-stress yield locus, such as Fig.2.3 anisotropic yielding results in distortion of the yield ellipse as shown in Fig.2.3 which represents the yield locus for highly textured titanium alloy sheet.

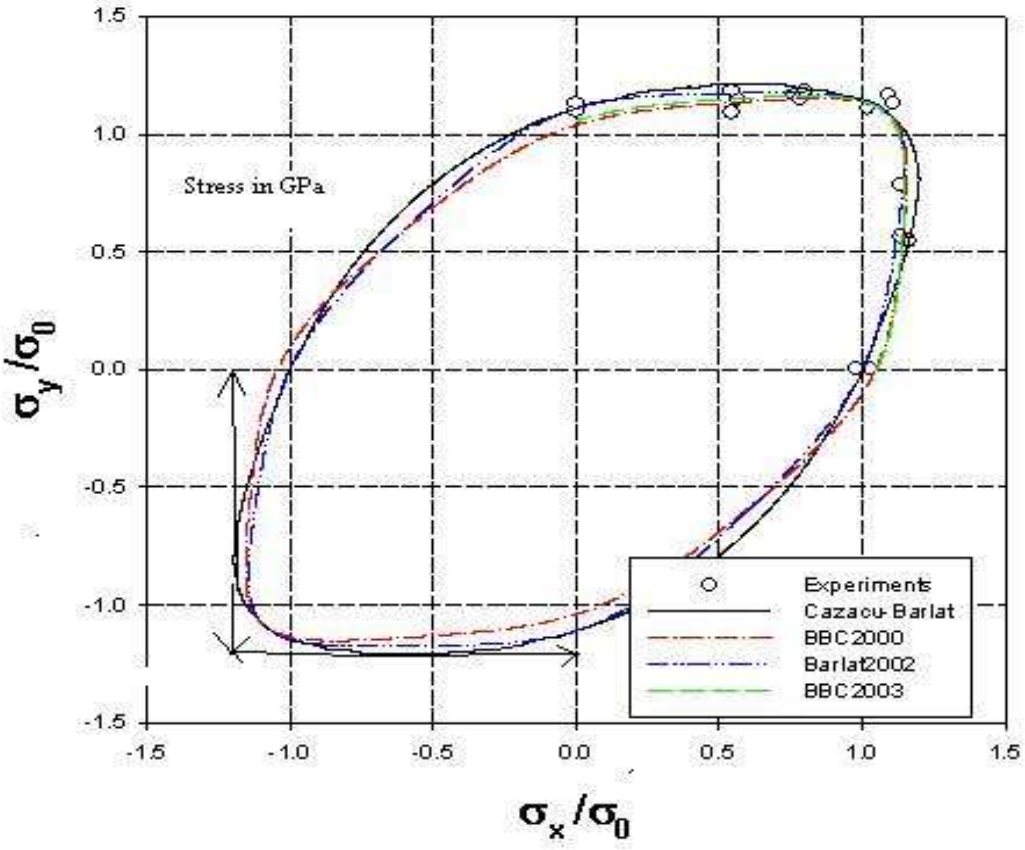

Fig 2.3 Yield locus for textured titanium-alloy sheet

2.2.4 Hoffman Yield Criterion

Hoffman [7] has proposed a fracture condition for orthotropic brittle materials using nine material parameters, which accounts for the differing yield strength under compression and tension in various directions. The condition has been subsequently used as a yield criterion for anisotropic materials by various investigators. In its original form, the Hoffman criterion takes anisotropy also into account and could be stated in terms of principal stresses as,

$$C_1(\sigma_{22}-\sigma_{23})^2+C_2(\sigma_{33}-\sigma_{11})^2+C_3(\sigma_{11}-\sigma_{22})^2+C_4\sigma_{11}+C_5\sigma_{22}+C_6\sigma_{33}+C_7\sigma_{23}^2+C_8\sigma_{31}^2+$$

$$C_9\sigma_{12}^2-1=0 \qquad (2.10)$$

In the principal stress space, the criterion simplifies to,

$$C_1(\sigma_{22}-\sigma_{23})^2+C_2(\sigma_{33}-\sigma_{11})^2+C_3(\sigma_{11}-\sigma_{22})^2+C_4\sigma_{11}+C_5\sigma_{22}+C_6\sigma_{33}-1=0 \qquad (2.11)$$

The Hoffman Yield Criterion [7] has been developed by borrowing feature from Von Mises isotropic yield condition and Hill anisotropic yield criterion. This criterion reduces to Hill criterion [6] by setting $C_4=C_5=C_6=0$, in eqn. (2.11), and when in eqn. (2.11) $C_1=C_2=C_3$ and, $C_4=C_5=C_6=0$ the criterion reduces to Von Mises surface [6] in the principal stress space.

2.3 Creep Laws

Several workers have proposed different laws which correlate effective stress to effective strain rate. Norton has proposed that effective strain ($\bar{\varepsilon}$) is related to applied stress (σ) by a power law relation of the following form:

$$\bar{\varepsilon} = A\sigma^{n_a}\exp(-Q_a/RT)$$

where, $\bar{\varepsilon}$ is the steady state creep rate, A is the constant sensitive to microstructure, σ is the applied stress, n_a is the apparent stress exponent, Q_a is the apparent activation energy, R is the gas constant and T is the absolute temperature. Norton's law has been widely criticized because of following two reasons [8],

(i) Firstly, the stress dependence of the creep rate, as described by the value of the stress exponent, n_a is anomalously high and ranges from about 10 to 75.

(ii) Secondly the temperature dependence of the creep rate measured in terms of creep activation energy, Q_a is often much larger than that for lattice self-diffusion.

In order to rationalize the strong stress and temperature dependency of creep rate, reported for the discontinuously reinforced, aluminum matrix composites, the concept of an effective stress has been developed. In this respect the power law creep equation as given above can be modified as,

$$\bar{\varepsilon} = A'[(\bar{\sigma}-\sigma_0)/E]^n\exp(-Q/RT)$$

where $\bar{\varepsilon}$ is the effective creep rate, A' is the structure dependent parameters, $\bar{\sigma}$ is the

applied stress , σ_0 is the threshold stress, n is the true stress exponent, E is the temperature-dependent Young's Modulus, Q is the true activation energy, R is the gas constant and T is the absolute temperature.

It has been pointed out that the creep behavior of aluminum alloys and their composites is related to modified creep behavior of solid solution alloys [8]. Thus, the equation developed for solid solution alloys can be used to describe the creep behavior of composites provided that the applied stress is replaced by an effective stress. The true stress exponent n is usually selected as 3, 5 and 8. These values of n correspond to three well-documented creep cases for metal and alloys: n=3 for creep controlled by viscous glide processes of dislocation, n=5 for creep controlled by high-temperature dislocation climb and n=8 for lattice diffusion-controlled creep with a constant structure [9].

2.4 Constitutive Equations for Creep under Multiaxial Loading

The treatment for multiaxial creep in isotropic material begins with well-known Levy-Mises equation [10] in principal stress space as given below,

$$d\varepsilon_1 = \frac{d\bar{\varepsilon}}{\bar{\sigma}}[\sigma_1-(\sigma_2+\sigma_3)/2]$$

$$d\varepsilon_2 = \frac{d\bar{\varepsilon}}{\bar{\sigma}}[\sigma_2-(\sigma_1+\sigma_3)/2] \qquad (2.12)$$

$$d\varepsilon_3 = \frac{d\bar{\varepsilon}}{\bar{\sigma}}[\sigma_3-(\sigma_1+\sigma_2)/2]$$

where, $d\varepsilon_1$, $d\varepsilon_2$ and $d\varepsilon_3$ indicate increments of plastic strain components, $\bar{\sigma}$ is the effective stress and $d\bar{\varepsilon}$ is the effective strain increments.

The effective stress, $\bar{\sigma}$, and strain increment, $d\bar{\varepsilon}$, are given by,

$$\bar{\sigma} = \frac{1}{\sqrt{2}}[(\sigma_2-\sigma_3)^2+(\sigma_3-\sigma_2)^2+(\sigma_1-\sigma_2)^2]^{1/2}$$

$$d\varepsilon = \frac{\sqrt{2}}{3}\ [(d\varepsilon_1 - d\varepsilon_2)^2 + (d\varepsilon_2 - d\varepsilon_3)^2 + (d\varepsilon_3 - d\varepsilon_1)^2]^{1/2}$$

Replacing the strain increments by strain rates in eq (2.12) to obtain,

$$\dot{\varepsilon}_1 = \frac{\bar{\varepsilon}}{\bar{\sigma}}\ [\sigma_1 - (\sigma_2 + \sigma_3)/2]$$

$$\dot{\varepsilon}_2 = \frac{\bar{\varepsilon}}{\bar{\sigma}}\ [\sigma_2 - (\sigma_1 + \sigma_3)/2]$$

$$\dot{\varepsilon}_3 = \frac{\bar{\varepsilon}}{\bar{\sigma}}\ [\sigma_3 - (\sigma_1 + \sigma_2)/2] \qquad (2.13)$$

The set of eqn. (2.13) are known as the constitutive equations for creep in an isotropic material in principal stress space.

2.5 Rotating Disc and Creep

Rotating disc [11] is an early invention during progress of civilization and provides an area of research and studies intensively pursued due to their vast utilization in rotating machinery namely turbine rotors, compressors, flywheels, disc brakes of automobiles and gears, computer disc drives etc. Optimal and more reliable design of rotating discs has long been an important issue in engineering design since very long. By changing suitably the geometrical parameters and physical properties, the optimal and more reliable design of a rotating disc for given operating conditions (i.e. load, speed, operating temperature) can be achieved.

Discs of gas turbines, jet engines and automotive and aerospace braking systems are usually operated at relatively higher angular speeds and subjected to high temperature/thermal gradient. Therefore, the prediction of long term steady state creep deformations is very important for these applications. A reduced weight of such components, resulting from the use of aluminum/ aluminum base alloys, is expected to save power and fuel due to a reduction in the payload. However, the enhanced creep of aluminium/aluminium alloys may not permit their use in such applications. Ceramic

reinforced aluminium/aluminium matrix composites have shown superior high temperature properties, therefore may be used for rotating disc applications exposed to elevated temperature [11].

Wahl et al., [12] have theoretically studied steady state creep deformation in a rotating turbine disc made of 12% chromium steel at 1000 ^{0}F using Von Mises and Tresca yield criteria and validated their results experimentally. They have described creep behavior by a power function relation of the following form,

$$\dot{\varepsilon} = k\,\sigma^n\, f\,(t)$$

where, $\dot{\varepsilon}$ is the strain rate, n and k are constants and $f\,(t)$ is a function of time. It is observed that the creep deformations obtained using Von Mises theory are too low compared to experimental results, which may be attributed to the anisotropy of the material used.

Ma [13] has used maximum shear stress theory to analyze creep deformations and stresses in a metallic gas turbine rotating solid disc of variable thickness, exposed to isothermal condition at elevated temperature, using maximum shear stress theory. The steady state creep in the disc is assumed to be the product of a power or exponential function of stress, multiplied by a function of time and another function of temperature. The analysis is extended for gas turbine and jet engine disc to demonstrate that the stress distributions over central portion of the disc having variable thickness are quite different from those observed in a disc of constant thickness [14]. The exponential creep law is used to describe steady state creep. Ma [15, 16] has further extended his analysis for disc having variable thickness and operating under a temperature gradient in the radial direction of the disc. In these different analyses, steady state creep is described by either exponential creep law [15] or power law creep [16] and closed form solutions are obtained for creep stresses.

Arya and Bhatnagar [17] have carried out creep analysis of orthotropic rotating disc using constitutive equations and a time hardening law. It is reported that the tangential stress at any radius and the tangential strain rate at the inner radius decrease with increasing anisotropy of the material.

Jerzy Biakiewicz [18] has presented a theoretical analysis of the finite strains in a rotating discs followed by damage and creep rupture front motion as described by Kachanov's hypothesis. The creep is represented by the generalized Norton-Odqvist law for the true stresses and logarithmic strains. An iterative method of solution is proposed. The analysis allows for the inclusion of inertia forces in the formulation of equilibrium.

Bhatnagar et al [19] have performed steady state creep analysis of orthotropic rotating discs having constant thickness, linearly varying thickness and hyperbolically varying thickness. They have used Norton's power law to describe creep behavior of the disc material. It is concluded that by selecting a certain type of material anisotropy and an optimum profile for the disc, the stresses in the disc may be reduced, thereby leading to longer service life.

Durodola and Attia [20] have explored the potential benefits of using fiber reinforced, functionally graded materials for rotating hollow and solid discs. Creep results have been obtained for several forms of gradation with the same nominal volume fraction of reinforcement. This establishes a basis for comparison of results obtained for the different cases. The functionally graded material has been modeled as a non-homogeneous orthotropic material. The finite element method and direct numerical integration of the governing differential equations have been used to predict stress and deformation distribution in the discs.

Gupta *et al* [21] have obtained creep stresses and strain rates in thin rotating disc having variable thickness and variable density by using Seth's transition theory. It is observed that a rotating disc whose density and thickness ratio decreases radially is on the safer side of the design in comparison to a flat disc having variable density.

Singh [22] has investigated the effect of reinforcement-size, content and operating temperature on the steady state creep behavior in a rotating isotropic disc made of aluminum silicon carbide particulate composite, using Norton's creep law and Von Mises yields criterion. The study reveals that parameters such as particle size, particle content and temperature do not have significant effect on radial stress distribution but their effect on tangential stress is sizeable. However, the radial and tangential strain rates in the disc

decrease by several orders with decreasing particle size, increasing particle content and decreasing operating temperature.

Singh and Ray [10] have estimated steady state creep response in a rotating isotropic FGM disc without thermal gradient using Norton's power law. The disc is assumed to have linear variation of silicon carbide particles along the radial distance in a matrix of aluminum. It is concluded that, in a rotating isotropic FGM disc with linearly decreasing particle content from the inner to the outer radius, the steady state creep response in terms of strain rates is significantly superior compared to that in a disc with the same total particle content distributed uniformly.

Singh and Ray [23] have performed creep analysis in an anisotropic 6061Al-20 *wt%* SiC_w composite disc rotating at 15,000 *rpm* and undergoing steady state creep at 561 *K* following Norton's power law. The effect of anisotropy induced presumably by processing or inhomogeneous distribution of reinforcements has been investigated. The presence of anisotropy leads to significant reduction in the tangential and radial strain rates over the entire disc. Anisotropy appears to help in restraining creep response both in the tangential and in the radial directions. Increasing the strength of disc in tangential direction changes the nature of radial strain rate from small compressive to small tensile in the middle of the disc, which may cause unwanted deformations in shape of the disc. However, the effect of anisotropy on the tangential and radial stress is relatively small. The tangential stress in the anisotropic disc is lower in the middle of the disc but higher near the inner and the outer radii of the disc compared to that observed in an isotropic disc. The radial stress in the anisotropic disc is higher near the inner radius but lower near the outer radius with respect to that in an isotropic disc.

Jahed and Bidabadi [24] have presented a general axisymmetric method by extending the previously proposed variable material properties (VMP) method for analysis of primary and secondary creep in axisymmetric problem of rotating discs and pressure vessels. The method uses the basic solution for a rotating uniform isotropic disc and generates the solution for non-uniform inhomogeneous one. Primary and secondary creep behavior have been predicted using the proposed method and the results are compared to FEM solutions.

Singh and Ray [7] have analyzed steady state creep in an anisotropic composite disc showing Bauschinger effect, using Norton's power law and newly proposed yield criterion which, at appropriate limits, reduces to Hill anisotropic and Hoffman isotropic yield criterion. The new yield criterion results in significant changes in the tangential stress distribution but similar radial stress distributions in disc with residual stress compared to those obtained in a similar disc without residual stress following Hill's yield criterion. The presence of tensile residual stress in the disc is observed to increase the creep rate significantly compared to that in a similar anisotropic disc without residual stress.

Gupta et al [25] have analyzed the creep behavior of a rotating disc having constant thickness and made of isotropic functionally graded material (FGM).The disc under investigation is made of composite containing silicon carbide particles in a matrix of pure aluminum. The creep behavior has been described by Sherby's law. The disc is assumed to have a thermal gradient in the radial direction. The study indicates that for the assumed linear particle distribution, the steady-state strain rates in FGM disc are significantly lower compared to that in an isotropic disc with uniform particle distribution. It is also noticed that the strain rates in composite discs operating under thermal gradient are reduced compared to similar discs under a uniform average temperature.

Gupta et al [11] have analyzed steady state creep in an isotropic aluminum silicon carbide particulate rotating disc. The creep behavior has been described by Sherby's law. It is observed that the tangential as well as radial stresses increase as one move from the inner towards the outer radius of the disc, reaches maximum before decreasing near the outer radius. Further, the stress distribution in the disc does not vary significantly for various combinations of material parameters and operating temperatures. The tangential as well as radial strain rates decrease on moving from the inner towards the outer radius of the disc but radial strain rate reaches a minimum somewhere near the middle region of the disc. The tangential as well as radial strain rates in the disc reduces significantly with reducing particle size, increasing particle content and decreasing operating temperature.

Singh and Ray [26] have studied the effect of thermal residual stress leading to Bauschinger effect, on the steady state creep behavior of a rotating disc made of 6061 Al-

20 vol.% SiCw composite using isotropic Hoffman yield criterion while describing the creep by Norton's power law. The results obtained are compared with those obtained using Von Mises criterion. The study reveals that stresses are not significantly affected due to presence of residual stress. However, tensile residual stress contributes to an increase in the tangential strain rate, particularly in the region near the outer radius of the disc when compared with the strain rate in the disc without residual stress. The radial strain rate, that is usually compressive, changes significantly due to presence of residual stress and becomes tensile in the middle of the disc.

Gupta et al [27] have analyzed creep behavior of a rotating FGM disc made of isotropic composite containing varying amounts of silicon carbide in the radial direction and operating in presence of a thermal gradient, also in the radial direction. The thermal gradient experienced by the disc is the result of braking action as estimated by FEM analysis. The variation of silicon carbide content has been so tailored as to contain larger amounts of particles in a highly stressed region. The creep behavior of the disc under stresses developing due to rotation has been determined following Sherby's law and compared with that of a similar disc following Norton's law. The difference in the distribution of stresses and strain rates in the discs does not follow any definite trend but the values are somewhat different. The presence of thermal gradient and a linear particle gradient separately or their simultaneous presence result in a significant decrease in steady state creep rates as compared to that in a composite disc with the same average particle content (20 vol. %) distributed uniformly and operating under isothermal condition.

CHAPTER 3

PROBLEM FORMULATION

Rotating discs have been receiving considerable attention due its wide range of engineering applications in rotating machinery including turbines, pumps, compressors, flywheels, braking system of automobiles, railway and aerospace, computer disc drives etc. In most of these applications, the disc is subjected to severe mechanical and thermal loadings as it has to operate at elevated temperatures. This makes the disc material undergo creep deformations. The excellent mechanical properties like high specific strength/stiffness and high temperature stability offered by aluminum/aluminum alloy based composites consisting of silicon carbide particles/whiskers or fibers make them appropriate material for use in rotating disc applications.

The review reveals that studies pertaining to creep behavior of rotating composite disc of constant thickness are available in literature. However, the studies related to creep behavior of a composite disc having variable thickness that too of composite materials are rather scant. It is noticed that by changing the disc profile the stresses in the disc may be reduced significantly. Therefore, it is decided to carry out a study pertaining to steady state creep behavior of a rotating composite disc having variable thickness. The objective of the study will be focused to investigate the effect of varying the disc profile for the same volume of the disc on the steady state creep behavior of the composite disc.

CHAPTER 4

MATHEMATICAL ANALYSIS OF CREEP

In this chapter a mathematical model to describe steady state creep beahviour of a rotating composite disc having variable thickness will be developed. The creep behaviour of the disc material has been described by Sherby's constitutive model. The model developed has been used to calculate the stress and strain rate distributions for composite having following disc profile:

(i) linearly varying thickness, and

(ii) hyperbolically varying thickness.

The results have also been obtained for a composite disc having constant thickness for comparison. The volume of all the disc has been kept equal. The material of the disc is assumed to yield following Hill's anisotropic yield criterion. The anisotropy induced may be attributed to processing, such as forging, rolling or extrusion of the disc material, which often results in alignment of reinforcement.

4.1 Assumptions

For the purpose of analysis the following assumptions are made:

(1) Material of the disc is orthotropic and incompressible, i.e.

$$\dot{\varepsilon}_r + \dot{\varepsilon}_\theta + \dot{\varepsilon}_z = 0 \tag{4.1}$$

where the subscripts r, θ, and z refer to radial, tangential and axial directions respectively and the dot refers to differentiation with respect to time.

(2) Thickness of the disc is assumed to be very small compared to other dimensions, therefore axial stress in the disc may be assumed to be zero i.e.

$$\sigma_Z = 0 \tag{4.2}$$

Therefore, a condition of plane stress exists in the disc and the tangential and radial stresses are uniform across the thickness of the disc.

(3) Elastic deformations in the disc are small and therefore can be neglected compared to creep deformations.

(4) The composite shows a steady state creep behavior, which may be described by following Sherby's law of the form [7]

$$\bar{\varepsilon} = A_S \left[\frac{\bar{\sigma} - \sigma_0}{E} \right]^n$$

where, $\bar{\varepsilon}$ is the effective strain rate, $\bar{\sigma}$, the effective stress, n (=8) is the stress exponent, E the young's modulus and $A_S = \dfrac{AD_\lambda \lambda^3}{|b|^5}$ is a constant in which D_L is the lattice self-diffusion coefficient, λ is the subgrain size, $|b_r|$ is the Burgers vector, E is the young's modulus and A is a constant.

The above equation may be alternatively written as,

$$\bar{\varepsilon} = \left[M(\bar{\sigma} - \sigma_0) \right]^n \tag{4.3}$$

where the creep parameter $M = \dfrac{A_S^{1/n}}{E}$.

(5) Material of the disc yield according to Hill's criterion [7] as given by,

$$\bar{\sigma} = \left[\frac{1}{(G+H)} \left[F(\sigma_\theta - \sigma_z)^2 + G(\sigma_z - \sigma_r)^2 + H(\sigma_r - \sigma_\theta)^2 \right] \right]^{1/2} \tag{4.4}$$

where F, G and H are the anisotropic constant as described in section 2.2.3.

4.2 Analysis of Creep

Consider a thin orthotropic composite disc of 6061Al-SiC_W of density ρ and rotating at a constant angular speed ω. The disc thickness is assumed to be h and a and b be the inner and outer radii of the disc, respectively.

Let A and A_0 denote the areas of cross section of the discs having inner radius a but outer radii r and b respectively and say I and I_0 be respectively the moments of inertia of discs with outer radii r and b. Then one can write,

$$A = \int_a^r h dr,$$
$$A_0 = \int_a^b h dr,$$
$$I = \int_a^r h r^2 dr, \tag{4.5}$$
$$I_0 = \int_a^b h r^2 dr.$$

The average tangential stress in the disc, $\sigma_{\theta av}$ may be defined as,

$$\sigma_{\theta av} = \frac{1}{A_0} \int_a^b h \sigma_\theta dr \tag{4.6}$$

The constitutive equations for an orthotropic disc under multiaxial stress condition are given by as [11]:

$$\dot{\varepsilon}_r = \frac{\vec{\varepsilon}}{2\bar{\sigma}} \{(G+H)\sigma_r - H\sigma_\theta - G\sigma_z\}$$

$$\dot{\varepsilon}_\theta = \frac{\vec{\varepsilon}}{2\bar{\sigma}} \{(H+F)\sigma_\theta - F\sigma_z - H\sigma_r\} \tag{4.7}$$

$$\dot{\varepsilon}_z = \frac{\vec{\varepsilon}}{2\bar{\sigma}} \{(F+G)\sigma_z - G\sigma_r - F\sigma_\theta\}$$

where *F,G* and *H* are orthotropic constants of the material.

Since the material of the disc yield according to Hill's criterion given by,

$$\bar{\sigma} = \left[\frac{1}{(G+H)} \left[F(\sigma_\theta - \sigma_z)^2 + G(\sigma_z - \sigma_r)^2 + H(\sigma_r - \sigma_\theta)^2 \right] \right]^{1/2} \tag{4.8}$$

Due to symmetry of the disc,

u=u(r), v = w =0,

where u, v, w are radial, tangential and axial displacements, respectively.

In terms of displacement the strain rate in the disc may be written as,

$$\dot{\varepsilon}_\theta = \frac{\dot{u}}{r},$$
$$\dot{\varepsilon}_r = \frac{d\dot{u}}{dr} \tag{4.9}$$

Substituting value of $\bar{\varepsilon}$ and $\bar{\sigma}$ from equation (4.3) and (4.8) respectively, into the first equation amongst set of constitutive Eqs. (4.7), we get,

$$\frac{d\dot{u}_r}{dr} = \dot{\varepsilon}_r = \frac{\left[M\left(\bar{\sigma} - \sigma_0\right)\right]^n \left[(G+H)\sigma_r - H\sigma_\theta\right]}{2\left[\frac{1}{(G+H)}\{G{\sigma_r}^2 + F{\sigma^2}_\theta + H(\sigma_r - \sigma_\theta)^2\}\right]^{1/2}} \tag{4.10}$$

or

$$\frac{d\dot{u}_r}{dr} = \dot{\varepsilon}_r = \frac{\left[M\left(\bar{\sigma} - \sigma_0\right)\right]^n \left[(G+H)y - H\right]}{2\left[\frac{1}{(G+H)}\{Gy^2 + F + H(y-1)^2\}\right]^{1/2}} \tag{4.11}$$

where $y = \frac{\sigma_r}{\sigma_\theta}$, is the ration of radial and tangential stress.

Similarly, one may get from second equation from set of constitutive Eqs. (4.7),

$$\frac{\dot{u}_r}{r} = \dot{\varepsilon}_\theta = \frac{\left[M\left(\bar{\sigma} - \sigma_0\right)\right]^n \left[(H+F) - Hy\right]}{2\left[\frac{1}{(G+H)}\left\{F + Gy^2 + H(y-1)^2\right\}\right]^{1/2}} \tag{4.12}$$

and

$$\dot{\varepsilon}_z = -(\dot{\varepsilon}_r + \dot{\varepsilon}_\theta) \tag{4.13}$$

Dividing Eqn. (4.11) by (4.12), we obtain,

$$\frac{d\dot{u}_r}{dr} \cdot \frac{r}{\dot{u}_r} = \frac{(G+H)y - H}{(H+F) - Hy} \tag{4.14}$$

or

$$\frac{d\dot{u}_r}{dr} \cdot \frac{r}{\dot{u}_r} = \phi(r) \tag{4.15}$$

where

$$\phi(r) = \frac{(H+G)y - H}{(H+F) - Hy} \tag{4.16}$$

Eqn. (4.15) can be rewritten as,

$$\frac{d\dot{u}_r}{\dot{u}_r} = \phi(r)\frac{dr}{r}$$

On integrating above equation between limits *a* to *r*. One gets,

$$\dot{u}_r = \dot{u}_{ri} \exp \int_a^r \frac{\phi(r)}{r} dr \tag{4.17}$$

Dividing equation (4.17) by *r*, one gets $\dot{\varepsilon}_\theta$ which can be equated to Eqn. (4.12) to obtain,

$$\frac{\left[M\left(\overline{\sigma} - \sigma_0\right)\right]^n \left[(H+F) - Hy\right]}{2\left[\frac{1}{(G+H)}\left[F + Gy^2 + H(y-1)^2\right]\right]^{1/2}} = \frac{\dot{u}_{ri}}{r} \exp \int_a^r \frac{\phi(r)}{r} dr$$

The above equation may be simplified to obtain,

$$\overline{\sigma} - \sigma_0 = \frac{\dot{u}_{ri}}{M} \psi(r) \tag{4.18}$$

where

$$\psi(r) = \frac{2}{r}\left[\frac{\left(\frac{F + Gy^2 + H(y-1)^2}{(G+H)}\right)^{1/2}}{\left[(H+F) - Hy\right]} \exp\left[\int_a^r \frac{\phi(r)}{r} dr\right]\right]^{1/n} \tag{4.18a}$$

Substituting $\overline{\sigma}$ from Eqn. (4.8) into Eqn. (4.18), we get,

$$\left[\frac{1}{(G+H)}\left(Gy^2 + F + H(y-1)^2\right)\right]^{1/2} \sigma_\theta - \sigma_0 = \frac{(\dot{u}_{ri})^{1/n}}{M} \psi(r)$$

The above equation can be simplified to obtain σ_θ as,

$$\sigma_\theta = \frac{(\dot{u}_{ri})^{1/n}}{M} \psi_1(r) + \psi_2(r) \tag{4.19}$$

where,

$$\psi_1(r) = \frac{\psi(r)}{\left[\frac{1}{(G+H)}\left[Gy^2 + F + H(y-1)^2\right]\right]^{1/2}} \tag{4.20}$$

and

$$\psi_2(r) = \frac{\sigma_0}{\left[\frac{1}{(G+H)}\left[Gy^2 + F + H(y-1)^2\right]\right]^{1/2}} \tag{4.21}$$

4.3 Equilibrium Equation for Rotating Disc

Let us consider an element of the disc, as shown in Fig. 4.1, between radius *r* and (*r+dr)* and subtending an angle $d\theta$ at the centre of the disc 'O'. Say the thickness of the disc at radial distance *r* and (*r+dr)* be *h* and (*h+dh*) respectively.

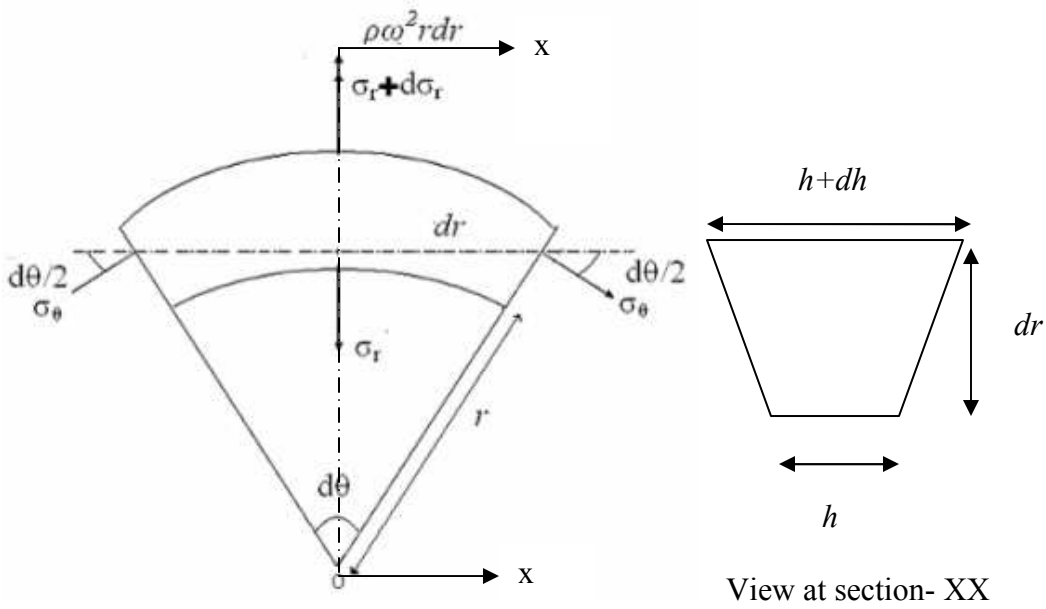

Fig. 4.1. Free body diagram of an element of the disc.

Resolving the forces acting on the disc element along the vertical direction, *i.e.* $\sum v = 0$ implies,

$$[\sigma_r + \frac{d\sigma_r}{dr} \cdot dr] \cdot [r + dr] \cdot [d\theta] \cdot [h + dh] - \sigma_r \cdot r \cdot d\theta \cdot h - [2 \cdot \sigma_\theta \cdot \frac{d\theta}{2}] \cdot [2h + dh] \cdot \frac{dr}{2}$$
$$+ \rho \cdot r \cdot \omega^2 [2h + dh] \cdot [r + \frac{dr}{2}] \cdot [\frac{dr}{2}] \cdot d\theta = 0$$

Neglecting the smaller term from above equation and simplifying, we get

$$\frac{d}{dr}[\sigma_r \cdot r \cdot h] - \sigma_\theta \cdot h - \rho \cdot r^2 \cdot \omega^2 \cdot h = 0 \qquad (4.22)$$

The above equation is the equation of equilibrium for the rotating disc of variable thickness.

Integrating Eqn. (4.22) between limits *a* to *b*, we get,

$$[h \cdot r \cdot \sigma_\theta]_a^b - \int_a^b h \cdot \sigma_{\theta \cdot} \cdot dr + \rho \cdot \omega^2 \int r^2 \cdot h \cdot dr = 0$$

or

$$[h_b \cdot b_b \cdot \sigma_{rb} - h_a \cdot b_a \cdot \sigma_{ra}] - \int_a^b h \cdot \sigma_{\theta \cdot} \cdot dr + \rho \cdot \omega^2 \cdot I_0 = 0 \qquad (4.23)$$

where I_0 is given by Eqn. (4.5).

Dividing Eqn. (4.23) by A_0, and rearranging the terms we can get the average tangential stress, defined in Eqn. (4.6), as,

$$\sigma_{\theta av} = \frac{1}{A_0} \int_a^b h \cdot \sigma_\theta .dr = \frac{h_b \cdot b \cdot \sigma_{rb}}{A_0} - \frac{h_a \cdot a \cdot \sigma_{ra}}{A_0} + \frac{\rho \cdot \omega^2 \cdot I_0}{A_0}$$

or

$$\sigma_{\theta av} = \frac{1}{A_0} \int_a^b h \cdot \sigma_\theta .dr = \frac{1}{A_0} \left[\rho \cdot \omega^2 \cdot I_0 - a \cdot h_a \cdot \sigma_{ra} + b \cdot h_b \cdot \sigma_{rb} \right] \qquad (4.24)$$

where, h_a and h_b denote the thickness of the disc respectively at the inner and the outer radii, and σ_{ra} and σ_{rb} are the radial stresses at the inner and outer radii respectively.

In the present analysis it is assumed that a free rotating orthotropic hollow disc, the radial stress, σ_r, must zero at the inner and the outer radii of the cylinder, thus

$$\begin{pmatrix} \sigma_{ra} = 0 \ at \ r = a \\ \sigma_{rb} = 0 \ at \ r = b \end{pmatrix} \qquad (4.25)$$

Substituting σ_θ from Eqn. (4.19) into Eqn. (4.6), one may write,

$$\sigma_{\theta av} = \frac{1}{A_0} \int_a^b \left(\frac{\dot{u}_{ri}^{1/n}}{M} \cdot \psi_1(r) + \psi_2(r) \right) \cdot h \cdot dr$$

The above equation can be simplified as,

$$\frac{\dot{u}_{ri}^{1/n}}{M} = \frac{A_0 \cdot \sigma_{\theta av} - \int_a^b \psi_2(r) \cdot h \cdot dr}{\int_a^b \psi_1(r) \cdot h \cdot dr}$$

Substituting $\sigma_{\theta av}$ from Eqn. (4.24) into above equation and simplifying one gets,

$$\frac{\dot{u}_{ri}^{1/n}}{M} = \frac{\left[\rho \cdot \omega^2 \cdot I_0 - a \cdot h_a \cdot \sigma_{ra} + b \cdot h_b \cdot \sigma_{rb}\right] - \int_a^b \psi_2(r) \cdot h \cdot dr}{\int_a^b \psi_1(r) \cdot h \cdot dr} \tag{4.26}$$

It is important to mention that the radial stresses σ_{ra} and σ_{rb} at the inner and the outer radii, respectively are zero due the imposed boundary conditions as given by Eqn.(4.25).

In the first iteration, it is assumed that $\sigma_\theta = \sigma_{\theta av}$ over the entire disc radii. The $\sigma_{\theta av}$ can be obtained from Eqn. (4.24) given above.

Substituting $\sigma_{\theta av}$ for σ_θ in the equilibrium Eqn. (4.22), and integrating within limits *a* to *r*, the first approximation for σ_r can be obtained as,

$$\left[h \cdot r \cdot \sigma_r\right]_a^r - \int_a^r h \cdot \sigma_\theta \cdot dr + \rho \cdot \omega^2 \int_a^r r^2 \cdot h \cdot dr = 0$$

Using the boundary conditions given by Eqn. (4.25) into above equation, we may obtain radial stress as,

$$\sigma_r = \frac{1}{h \cdot r}\left[\int_a^r \sigma_\theta \cdot h - \rho \cdot \omega^2 \cdot I\right] \tag{4.27}$$

Where the term *I* has been already defined in Eqn. (4.5).

Knowing σ_r *and* σ_θ, the stress ratio, $y = \frac{\sigma_r}{\sigma_\theta}$ can be calculated and hence second approximation for σ_θ, may be calculated from Eqn. (4.19) which can be again used to in Eqn. (4.27) to obtain the second approximation of σ_r. The process is carried out till the convergence in achieved. Once the distributions of radial and tangential stress are known, the strain rates in the disc may be calculated from Eqs. (4.11) and (4.12).

4.4. Disc Profiles

In this study we have considered following two different profiles of the disc:

(i) Disc with linearly varying thickness, Fig. (4.2), given by,

$$h = h_b + 2*C*(b-r) \tag{4.28}$$

Taking the thickness of the disc at the inner radius, h_a, and at the outer radius, h_b, as 1.44 *mm* and 0.75 *mm* respectively, the value of constant C appearing in Eqn. (4.28) comes out to be 0.002859.

(ii) Discs with hyperbolically varying thickness, Fig. (4.2), given by,

$$h = C_1 r^m , \tag{4.29}$$

The thickness of this disc at the inner and the outer radius are taken as 2.42 *mm* and 0.76 *mm* respectively, therefore the values of C_1 and m appearing in Eqn. (4.29) are calculated as 31.26 and -0.74 respectively.

It is important to mention here that the thickness of both the discs at the inner and the outer radii are selected in such a manner that both the disc has same volume. For the purpose of comparison, the results has also been calculated for disc having uniform thickness of 1 *mm* but having the volume same as that of linearly varying and hyperbolically varying thickness. The inner and the outer radii of all the discs are taken as 31.75 *mm* and 152.4 *mm* respectively.

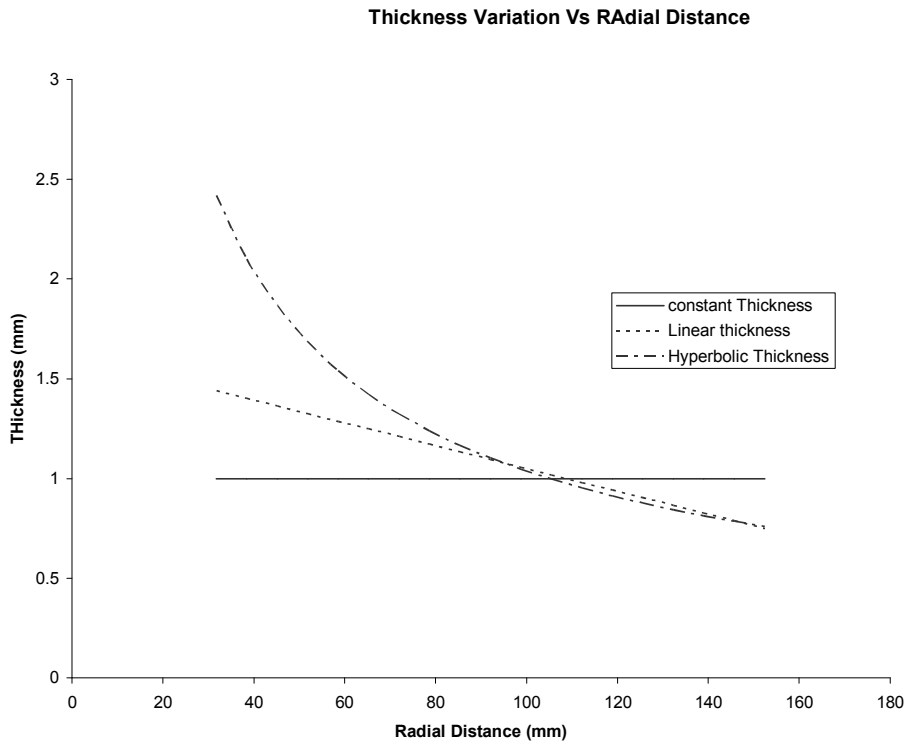

Fig.4.2. Variation of disc thickness with radial distance for different discs

4.5. Calculation of Area and Inertia of Discs

Using Eqs. (4.28) and (4.29) in Eqn. (4.5) the values of *A, A_0, I* and I_0 may be calculated. The values obtained are given as below,

(i) Disc having linearly varying thickness:

$$A = (r-a)[h_b + C*(2*b-r-a)] \tag{4.30}$$

$$A_0 = (b-a)[h_b + C*(b-a)] \tag{4.31}$$

$$I = h_b \cdot (\frac{r^3-a^3}{3}) + 2*C*b\cdot(\frac{r^3-a^3}{3}) - C*(\frac{r^4-a^4}{2})] \tag{4.32}$$

$$I_0 = h_b \cdot (\frac{b^3-a^3}{3}) + 2*C*b\cdot(\frac{b^3-a^3}{3}) - C*(\frac{b^4-a^4}{2})] \tag{4.33}$$

(ii) Disc having hyperbolically varying thickness:

$$A = C\cdot(\frac{r^{m+1}-a^{m+1}}{m+1}) \tag{4.34}$$

$$A_0 = C(\frac{b^{m+1}-a^{m+1}}{m+1}) \tag{4.35}$$

$$I = C(\frac{r^{m+3}-a^{m+3}}{m+3}) \tag{4.36}$$

$$I_0 = C(\frac{b^{m+3}-a^{m+3}}{m+3}) \tag{4.37}$$

The values of *A, A_0, I* and I_0 obtained above for the discs having variable profile may be used in the analysis described in section-4.3 to calculate the stress and strain rate distributions in the different discs.

4.6. Creep Parameters

The parameters *M* and σ_0 appearing in the Sherby's law describing steady state creep behaviour as given in Eqn. (4.3), are dependent on the material, be it monolithic or composite. These parameters are also affected by temperature. In a composite, the dispersoid size and the percentage of the dispersed particles or fibers are the primary variables determining these parameters. The values of *M* and σ_0 have been obtained regression equation developed by Gupta *et al* [29] from the experimental results reported

for 6061Al-$SiC_{P,W}$ (subscript 'P' implies particle and 'W' implies whisker form of SiC reinforcement). In this study the parameters M and σ_0 have been taken as 7.5×10^{-3} $s^{1/8}/MPa$ and 34.12 MPa respectively. The reported values of the creep parameters correspond whisker size 14.5 μm, whisker content = 30 *vol%* and operating temperature = 623 K.

4.7. Anisotropic Constants

The anisotropic constants, *F. G and H* appearing in Hill's yield criterion given by Eqn. (4.4) has been obtained from following equations as given in chapter-2.

$$G+H=\frac{1}{x^2}$$

$$H+F=\frac{1}{y^2} \qquad (4.38)$$

$$F+G=\frac{1}{z^2}$$

Where x, y and z are the yield stresses in the principal directions r, θ and z of the disc.

It is assumed that the material of the disc 6061Al-SiC_W contains SiC whisker aligned in the tangential (θ) direction due to processing. Therefore, the θ-direction has been taken as the longitudinal direction and the other two directions i.e. r and z have been taken as the transverse direction. In a rotating disc assuming the directions r, θ and z as the principal directions, the anisotropic constants as given by Eqn. (4.38), may be expressed as,

$$2F = \left(\frac{1}{\sigma_{\theta_Y}^{\ 2}} + \frac{1}{\sigma_{z_Y}^{\ 2}} - \frac{1}{\sigma_{r_Y}^{\ 2}} \right)$$

$$2G = \left(\frac{1}{\sigma_{z_Y}^{\ 2}} + \frac{1}{\sigma_{r_Y}^{\ 2}} - \frac{1}{\sigma_{\theta_Y}^{\ 2}} \right) \qquad (4.39)$$

$$2H = \left(\frac{1}{\sigma_{r_Y}^{\ 2}} + \frac{1}{\sigma_{\theta_Y}^{\ 2}} - \frac{1}{\sigma_{z_Y}^{\ 2}} \right)$$

where, $\sigma_{r_Y}, \sigma_{\theta_Y}$ and σ_{z_Y}, are the yield stresses of the composite in *r,* θ and z directions respectively. In the present study, it is assumed that σ_{r_Y} and σ_{z_Y} are the yield stresses in transverse direction have the same value σ_{T_Y}, and σ_{θ_Y}, the yield stress in the longitudinal direction is σ_{L_Y}. Therefore, Eqn. (4.39) becomes,

$$F = H = \frac{1}{2}\left[\frac{1}{\sigma_{L_Y}^{\ 2}} \right] \quad \text{and} \quad G = \frac{1}{2}\left[\frac{2}{\sigma_{T_Y}^{\ 2}} - \frac{1}{\sigma_{L_Y}^{\ 2}} \right] \tag{4.40}$$

The longitudinal yield stress, σ_{L_Y}, and the transverse yield stress, σ_{T_Y}, for the composite can be obtained using rule of mixture and inverse rule of mixture, respectively, as given below [30],

$$\sigma_{L_Y} = \sigma_{m_Y}(1 - V_f) + \alpha \sigma_{f_Y} V_f \tag{4.41}$$

and,

$$\frac{1}{\sigma_{T_Y}} = \frac{V_m}{\sigma_{m_Y}} + \frac{\beta V_f}{\sigma_{f_Y}} \tag{4.42}$$

where, α and β are constants, V_f, the volume fraction of fiber, σ_{m_Y}, the matrix yield strength (= 275.8 *MPa* for 6061Al, [31]), and σ_{f_Y} is the fiber strength (= 2800 *MPa* for SiC_w, [32]).

The constants α and β have been calculated from Eqs. (4.41) and (4.42), respectively, by using the experimental values of yield strengths as measured by Badini [33] for extruded bars made of 6061Al alloy based composite reinforced with 15 *vol %* silicon carbide whiskers. The experimental yield strengths as noticed by Badini in the longitudinal and transverse directions are σ_{L_Y} = 218 *MPa* and σ_{T_Y} = 145 *MPa*, respectively. On substituting V_f = 0.15, σ_{L_Y} = 218, σ_{T_Y} = 145, σ_{m_Y} = 275.8 and σ_{f_Y} = 2800 in Eqs. (4.41) and (4.42), the constants α and β are evaluated as -0.039 and 71.21, respectively. The α

and β thus obtained have been substituted in Eqs. (4.41) and (4.42) to calculate the values of σ_{L_Y} and σ_{T_Y}, which on substituting in Eqn. (4.40) gives the values of anisotropic constant as $F=H=1.95\text{x}10^{-5}$, MPa^{-2} and $G=8.39\text{x}10^{-5}$ MPa^{-2}. These values are used in the analysis to carry out the numerical computations.

4.8. Solution Procedure

The stress distribution is evaluated from the above analysis by iterative numerical scheme of computation. In the first iteration, it is assumed that $\sigma_\theta = \sigma_{\theta av}$ over the entire disc radii. Substituting $\sigma_{\theta av}$ for σ_θ in Eqn. (4.27) the first approximation value of σ_r i.e. σ_{r1} is obtained. The first approximation of stress ratio, *i.e.* y_1, is obtained by dividing σ_{r1} by $\sigma_{\theta av}$, which can be substituted in Eqn. (4.16) to calculate first approximation of $\phi(r)$ i.e. $[\phi(r)]_1$. Now one carries out the numerical integration of $[\phi(r)]_1$ from limits of *a* to *r* and uses this value in Eqn. (4.18a) to obtain first approximation of $\psi(r)$ i.e. $[\psi(r)]_1$ Using this $[\psi(r)]_1$, in Eqn. (4.20) and (4.21) respectively, $\psi_1(r)$ and $\psi_2(r)$ are found, which are used in Eqn. (4.19) to find second approximation of σ_θ i.e. $[\sigma_\theta]_2$. Using $[\sigma_\theta]_2$ for σ_θ in Eqn. (4.27), second approximation of σ_r i.e. $[\sigma_r]_2$ is found and then the second approximation of y i.e. $[y]_2$ is obtained. The iteration is continued till the process converges and gives the values of stresses at different points of the radius grid. The convergence was achieved in six to eight iterations. For rapid convergence 75 percent of the value of σ_θ obtained in the current iteration has been mixed with 25 percent of the values of σ_θ obtained in the last iteration for use in the next iteration. Since the problem has cylindrical symmetry the state of stress is now completely known under condition of creep. The strain rates are calculated now from the Eqs. (4.11)-(4.13).

The numerical solutions have been obtained for discs having (i) variable thickness, (ii) hyperbolically varying thickness and (iii) constant thickness.

CHAPTER 5

RESULTS AND DISCUSSIONS

Numerical calculations, based on the analysis presented in chapter-4 have been carried out to obtain steady state creep response of the composite disc of (i) variable thickness, (ii) hyperbolically varying thickness and (iii) constant thickness but all the disc have same volume. The material of the disc is assumed to be 6061Al-$SiC_{P,W}$ which undergo steady state creep following Sherby's creep law, Eqn. (4.3). The effect of disc profile has been investigated on the creep behavior of the isotropic (6061Al-SiC_P) and anisotropic disc (6061Al-SiC_W). In order to obtain the distributions of stresses and strain rates in the isotropic disc the values of anisotropic constant in the analysis given in chapter-4 has been set equal *i.e.* $F=G=H$. The effects of using different disc profiles on the creep behavior of the discs are discussed separately for the isotropic and anisotropic disc.

5.1. Effect of Disc Profile on Isotropic Disc

Figs. 5.1-5.4 show the effect of varying the disc thickness on the creep behavior of the composite disc made of isotropic material (6061Al- 30% *vol* SiC_P). The size of the SiC particles is kept 14.5 μm and the disc is assumed to operate at 623 K.

The tangential stress as shown in Fig. 5.1 increases on moving from the inner towards the outer radius of the disc, reaches a maximum before decreasing again at the outer radius. The tangential stress in the disc having linearly varying thickness reduces over the entire disc radii when compared to composite disc having uniform thickness. The disc having hyperbolically varying thickness exhibits the lowest values of tangential stress over the entire radius compared to uniform or variable thickness disc. Therefore, it is evident that by increasing and decreasing the disc thickness respectively near the inner and the outer radii, compared to uniform thickness, the tangential stress in the disc could be reduced to a significant extent.

The radial stress as shown in Fig. 5.2, increases from zero at the inner radius, reaches maximum before dropping to zero again at the outer radius under the imposed boundary conditions of radial stress vanishing at both the inner radius and the outer radius.

The radial stress in the disc with linearly varying thickness is reduced everywhere compared to disc of uniform thickness. The disc having hyperbolically varying thickness has radial stress lower than the uniform thickness disc but a little higher radial stress than the disc with linearly varying thickness near the inner radius of the disc. However, towards the outer radius the radial stress in disc with hyperbolic profile is the highest. Fig. (5.3) depicts the effect of disc profile on tangential strain rate. The tangential strain rate is highest inner radius and goes on decreasing on moving towards the outer radius. The tangential strain rates in the linearly varying disc and hyperbolically varying discs are reduced by almost 1 and 2 orders of magnitude respectively compared to those observed in uniform thickness disc. The distribution of strain rate is relatively more uniform in disc having variable thickness, which may be lead to the reduction in distortion of the disc.

The radial strain rate (compressive) shown in Fig. 5.4 is maximum at inner radius and goes on decreasing with radial distance up to a certain radial distance followed by an increasing trend towards the outer radius. The effect of disc profile on radial strain rate is similar to those observed in Fig. 5.3 on tangential strain rate.

From above discussion it appears that the strain rates in the disc can be significantly reduced by using disc with variable thickness having more thickness at the inner radius and lesser thickness at the outer radius as compared to disc having uniform thickness.

5.2. Effect of Disc Profile on Anisotropic Disc

The effect of varying the disc thickness on creep behavior of the composite disc made of anisotropic material (6061Al- 30% *vol* SiC_W) are shown in Figs. 5.5-5.8. The size of the SiC whisker in disc is also taken as 14.5 μm while the operating temperature is again kept 623 K.

The distribution of tangential stress in anisotropic disc as shown in Fig. 5.5 is significantly different from that observed in isotropic disc, Fig. 5.1. The tangential stress distribution in the isotropic uniform composite disc has a relatively flat peak in the middle of the disc, decreasing towards the inner and the outer radius, Fig. 5.1. When anisotropy is introduced in a uniform disc, the flat peak in the middle splits into two peaks of similar heights located towards the inner and the outer radii, and there is a minimum between these two peaks situated in the middle. From the comparison of Figs.5.1 and 5.5 it is concluded

that anisotropy appears to decrease the tangential stress in the middle region of the uniform composite disc but the stresses near both the ends of radius increase, particularly that around the outer radius. The tangential stresses in the disc having variable thickness are reduced over the entire radius when compared to uniform disc. The effect is similar to that observed in isotropic disc in Fig. 5.1.The effect of disc profile on radial stress in anisotropic disc, Fig. 5.6, is similar to those observed in Fig. 5.1 for disc made of isotropic composite.

The tangential and radial strain rates as shown in Figs. 5.7 and 5.8 respectively are significantly lower than that observed in isotropic disc, Figs. 5.3-5.4. The radial strain rate in the middle of the disc becomes tensile whereas near the inner and the outer radii the nature remains compressive, Fig. 5.8. By changing the disc profile the strain rates (both tangential and radial) in the anisotropic disc get reduced to several orders of magnitude compared to uniform disc. As an example, the tangential as well as radial strain rates in linear disc and hyperbolic disc are reduced respectively by almost 5 and 11 orders of magnitude when compared to disc having uniform thickness.

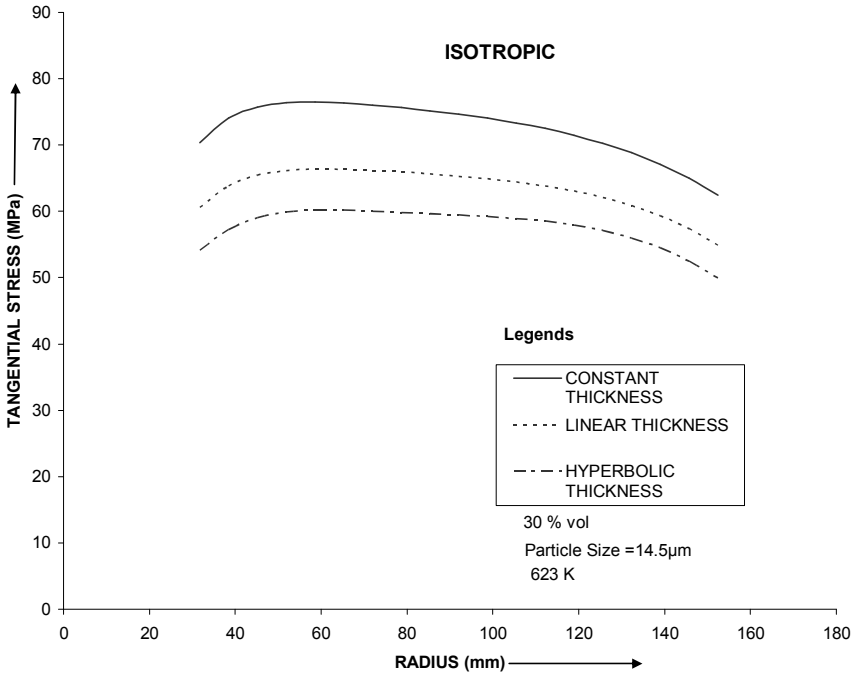

Fig.(5.1) Tangential stress versus radius for discs of the same volume but different profile

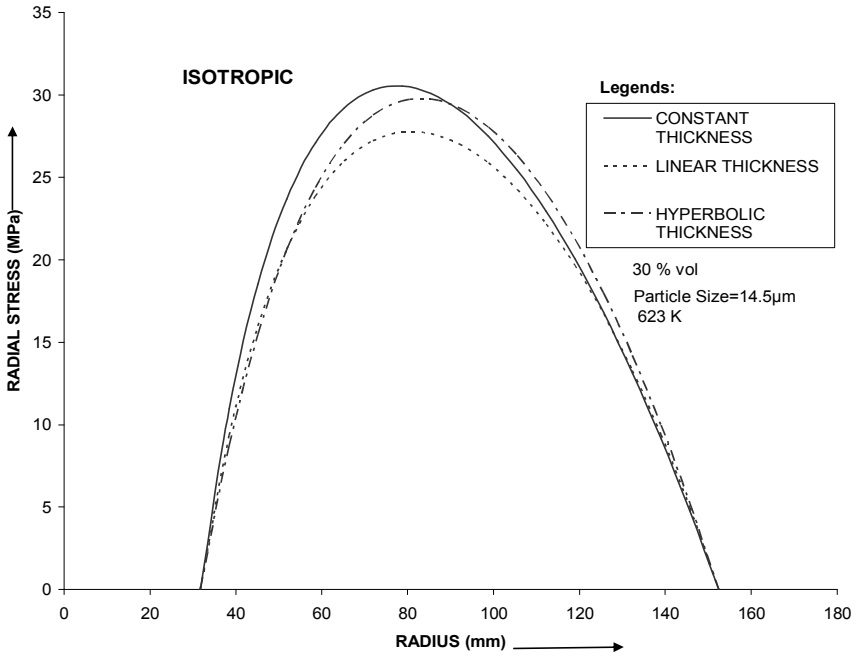

Fig (5.2) Radial stress versus radius for discs of the same volume but different profile

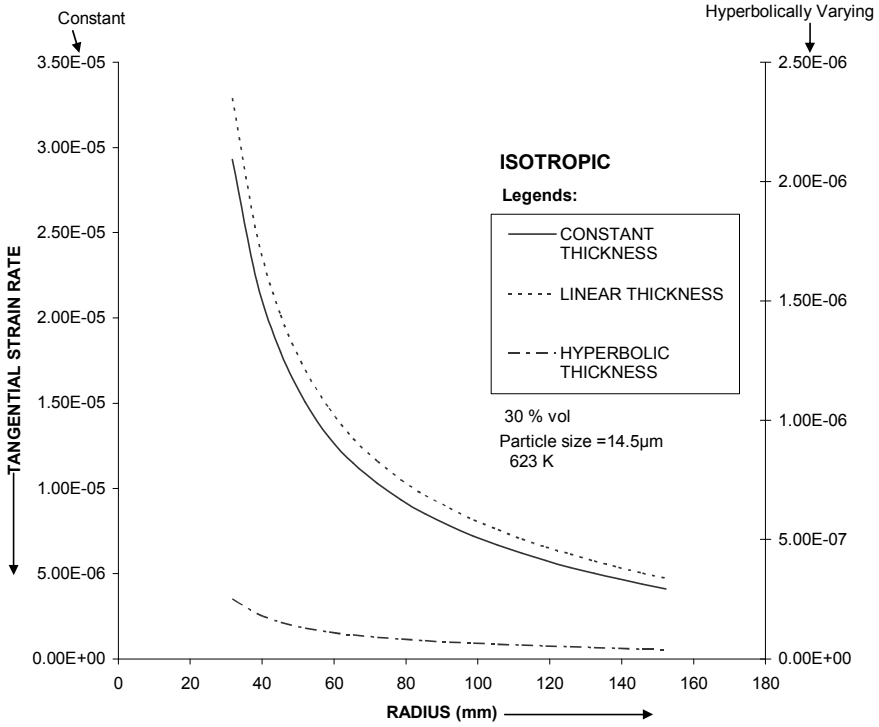

Fig. (5.3) Tangential strain rate versus radius for discs of the same volume but different profile

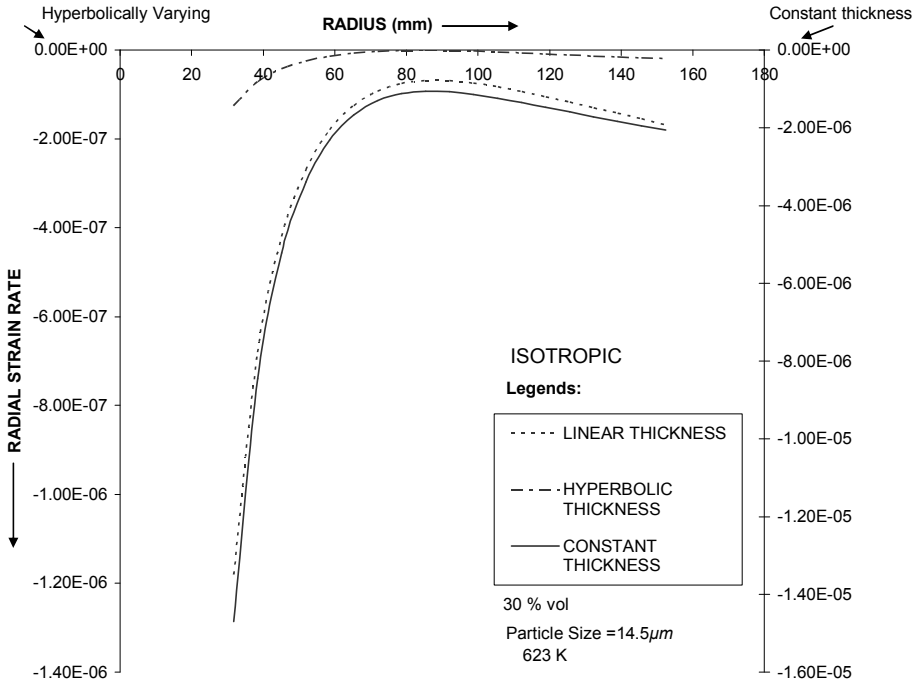

Fig.(5.4) Radial strain rate versus radius for discs of the same volume but different profile

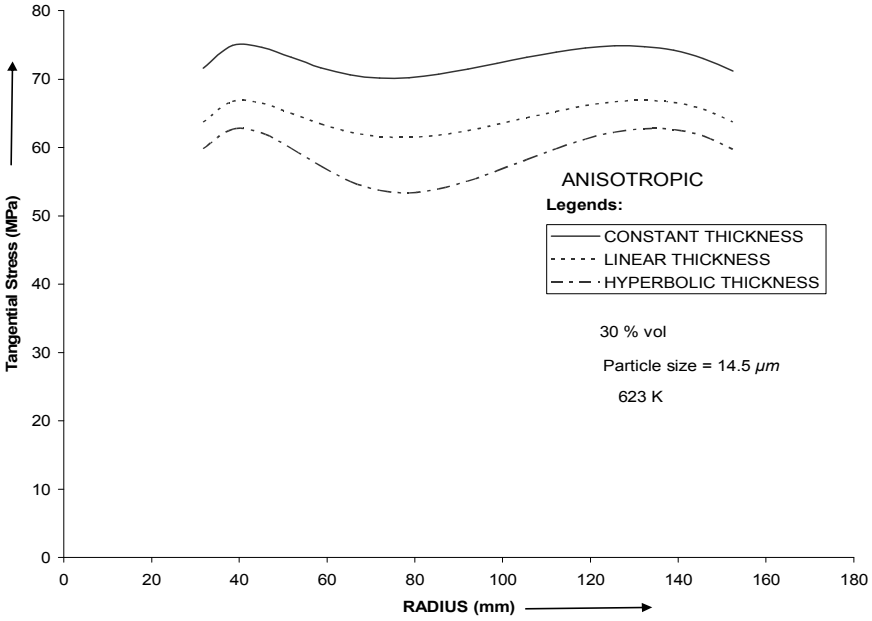

Fig.(5.5) Tangential stress versus radius for discs of the same volume but different profile

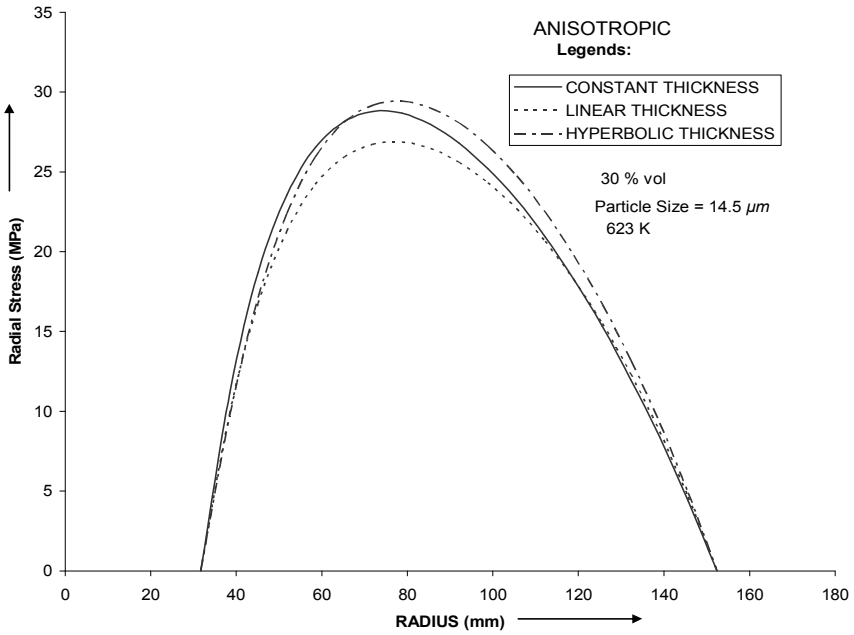

Fig (5.6) Radial stress versus radius for discs of the same volume but different profile

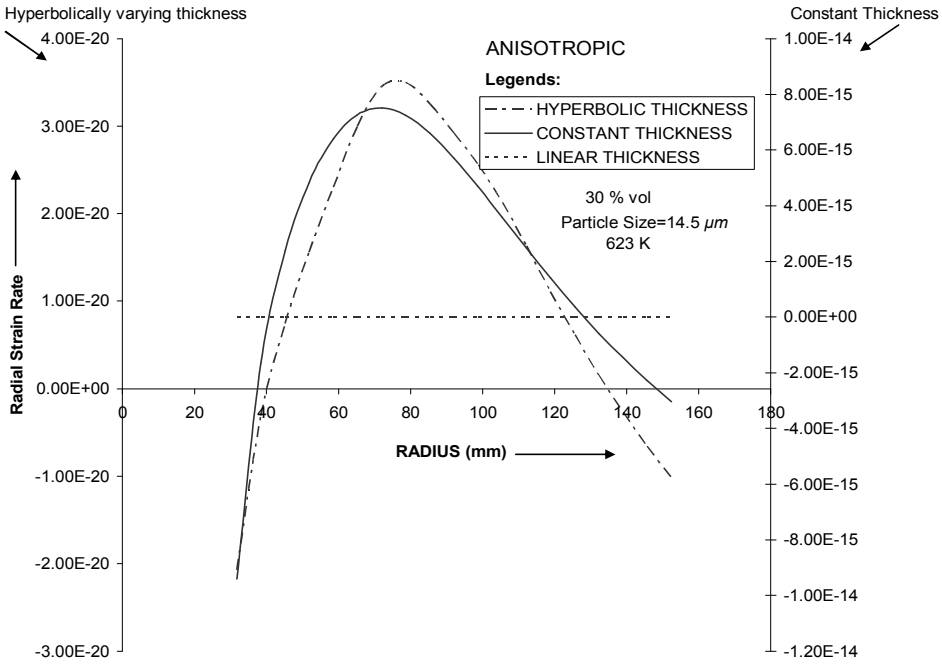

Fig.(5.7) Radial strain rate versus radius for discs of the same volume but different profile

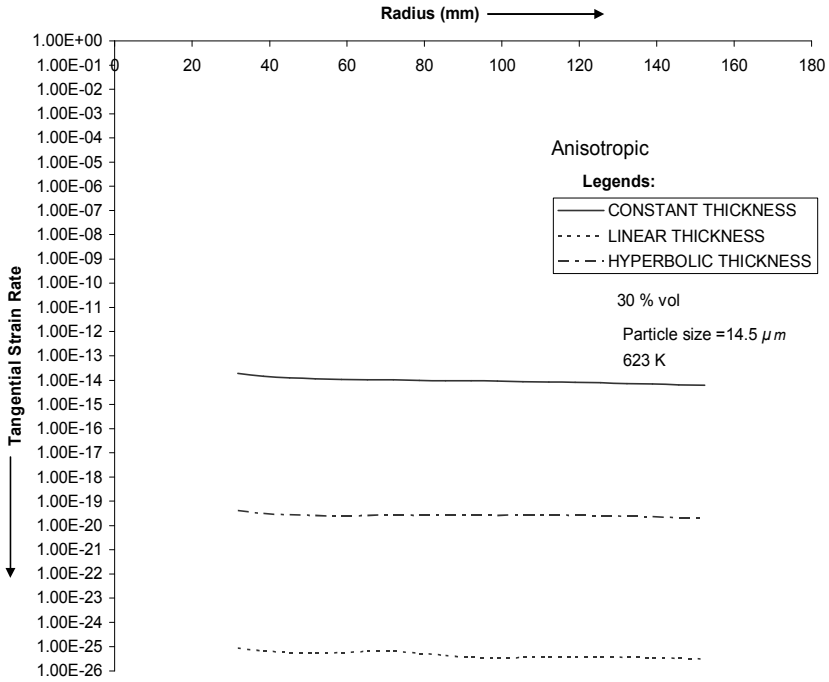

Fig. (5.8) Tangential strain rate versus radius for discs of the same volume but different profile

CHAPTER 6

CONCLUSIONS

Based on the results and discussion presented in chapter 5, the following conclusions are drawn:

1. The tangential stress in the disc could be significantly reduced by varying the disc profile. For the same disc volume and operating conditions, the tangential stress in the disc having linearly varying thickness are significantly lower than that observed in disc with either hyperbolic varying thickness or constant thickness.
2. The radial stress in the disc having linearly varying thickness are significantly lower over the entire radius compared to any other disc profile. However, the disc with hyperbolic profile exhibits relatively lower and higher stresses respectively near the inner and the outer radii, than that observed in uniform thickness disc.

3. The radial as well as tangential strain rates in the disc could be significantly reduced by employing disc with either hyperbolic or linear profile compared to uniform thickness disc. The disc having hyperbolic thickness profile has the lowest and more uniform distribution of strain rates. The effect of disc profile in much prominent in anisotropic disc than that observed in isotropic disc.

FUTURE SCOPE OF WORK

The study carried out in this thesis may be further extended in the following directions:

1. The analysis carried out in this work may be repeated for creep laws based on stress exponent n = 3 and 5, and its impact on the creep stress and steady state creep rates in a rotating disc may be investigated.
2. The study carried out in this thesis may be extended for disc operating under thermal gradients.
3. The effect of varying the disc profile may also be investigated for disc made of Functionally Graded Material.
4. Analysis may be repeated for disc having different boundary conditions e.g. in a turbine disc the blade effect may also be considered.
5. The creep response of rotating disc with other profiles and geometry may also be investigated.

REFERENCES

[1] http://www.wtec.org.

[2] Autar K. Kaw, "Mechanics of Composites Materials", CRC Press Boca Raton, New York, pp.2-18, 1997.

[3] V. K. Lindroos and M. J. Talvitie, "Recent Advances in Metal Matrix Composites", *Helsinki University of technology, Laboratory of Physical Metallurgy and Materials Science*,Finland,pp.274-279,1995.

[4] W. H. Hunt, Jr. "Metal Matrix Composites", *Aluminum Consultants Group, Inc., Murrysville*, PA, USA,pp.2-7,2000.

[5] M. Koizumi, "FGM activities in Japan", *Department of Materials Chemistry, Ryukoku University,* Ohtsu520-21, Japan, pp.2-4, 2002.

[6] George E. Deiter, "Mechanical Metallurgy", McGraw-Hill Book Company, Maryland, 1928.

[7] S. B. Singh and S. Ray , "Newly Proposed Yield Criteria for Residual Stress and Steady State Creep in an Anisotropic Rotating Composite Disc", *J. Mater Proc. Tech,* vol .143-144,pp.623-628,2003.

[8] S. C. Tjong and Z. Y. Ma, "Microstructural and mechanical Characteristics of in-situ Metal Matrix Composites", *Mater. Sci. Engg.*, A-29 pp. 49-113, 1999.

[9] Y. Li and T. G. Langdon, "An Examination of a Substructure-Invariant Model for the Creep of Metal Matrix Composites", *Mater. Sci. Engg*.,vol. 4 pp.276-284, 1999.

[10] S. B. Singh and S. Ray, "Steady-State Creep Behavior in an isotropic Functionally Graded Material Rotating Disc of Al-SiC Composite", *Metall. Trans*. vol.32, pp.1679-1685, 2001.

[11] V. K. Gupta, S. B. Singh, H. N. Chandrawat and S. Ray, "Steady State Creep and Material Parameters in a Rotating disc of Al-SiCp Composites", *European journal of Mechanics A/Solids*,vol.23,pp.335-344,2004.

[12] A. M. Wahl, G. O. Sankey, M. J. Manjoine, and E. Shoemaker, "Creep Tests of Rotating Disks at Elevated Temperature and Comparison with Theory", *J. Appl. Mech*, vol.21, pp.225-35, 1954.

[13] B. M. Ma, "A Creep Analysis of Rotating Solid Discs", *J .of the Franklin inst*., vol.267 (2), pp.167-168, 1959.

[14] B.M.Ma, "A further creep analysis for rotating solid disks of variable thickness", *Journal of the Franklin institute, vol. 269, pp 408-419, May 1960.*

[15] B.M.Ma, "Creep Analysis of Rotating solid discs with variable thickness and temperature", *Journal of the Franklin institute, vol. 270, pp 40-54, Jan.1961.*

[16] B.M.Ma, "A power-function creep analysis for rotating solid disks having variable thickness and temperature", *Journal of the Franklin institute, vol. 277, issue 6, pp 593-612, June 1964.*

[17] V. K. Arya and N. S. Bhatnagar, "Creep Analysis of Rotating Orthotropic Discs", *Nuclear Engg. Design*, vol.55, pp.323-330, 1979.

[18] Jerzy Bialkiewicz, "Dynamic Creep Rupture of a Rotating disc of Variable Thickness", *Int. J. Mech. Sci. Vol. 28, No. 10, pp. 671-681,1986.*

[19] N. S. Bhatnagar, P. S. Kulkarni and V. K. Arya, "Steady State Creep of Orthotropic Rotating Discs of Variable Thickness", *Nuclear Engineering and Design,* vol.91, pp. 121-141, 1986.

[20] J. F. Durodola amd O. Attia, "Deformation and Stresses in Functionally graded Rotating Discs", *Composites Science and Technology, Vol.60, pp. 987-995, June 1999.*

[21] S.K.Gupta, Sanjeev Sharma and Sonia Pathak, "Creep transition in a thin Rotating Disc having Variable Thickness and Variable Density", *Indian J. Pure appl. Math.,31(10):1235-1248*, 2000.

[22] S. B. Singh, "Flow Behavior and Creep Deformation in Engineering Components of Composites", Ph.D. Thesis, *University of Roorkee,* 2000.

[23] S. B. Singh and S. Ray, "Modeling the anisotropy and creep in orthotropic aluminum–silicon carbide composite rotating disc", *Mechanics of Materials, vol. 34, issue 6, pp. 363-372, Jun.2002*.

[24] H. Jahed and J. Bidabadi, "An Axisymmetric Method of Creep Analysis for Primary and Secondary Creep", *Int. J. Pressure Vessels Pipings*, vol.80, pp.597-606, 2003.

[25] V. K. Gupta, S. B. Singh, H. N. Chandrawat and S. Ray, "Creep Behavior of a Rotating Functionally Graded Composite Disc Operating under Thermal Gradients", *Metallurgical and Materials Transactions*, vol.35A, pp.1381-1391, 2004.

[26] S.B.Singh and S.Ray, "Modeling the Creep in an Isotropic Rotating Disc of Al-SiC_w Composite in Presence of Thermal Residual Stress", *Proc. 3rd International Conference on Advanced Manufacturing Technology: ICMAT-2004*, May 11-13, Kualalumpur, Malaysia, pp. 766-770, 2004.

[27] V. K. Gupta, S. B. Singh, H. N. Chandrawat and S. Ray, "Modeling of creep behavior of a rotating disc in the presence of both composition and thermal gradients", *Journal of Engg. Materials and Tech., vol.127, pp.97-105, Jan.2005.*

[28] A.B.Pandey, R.S.Mishra and Y.R.Mahajan, "Steady State Creep Behaviour of Silicon Carbide Particulate Reinforced Aluminium Composites," Acta Metall. Mater., Vol. 40(8), pp. 2045-2052., 1992.

[29] V.K.Gupta, "Modeling of Creep Behavior of Rotating Discs of Composite Materials", Ph.D. Thesis, *T.I.E.T, Patiala,* 2005.

[30] J.A.Jacobs and T.F.Kilduff, "Engineering Materials Technology (Structure, Processing, Properties and Selection)", 3rd Edition, Prentice Hall Int.,Inc., p. 559, 1997.

[31] D.E.Alman, "Properties of Metal-Matrix Composites", in: ASM Handbook, Vol. 21: Composites, ASM International, Metals Park, Ohio, pp. 838-858, 2001.

[32] T.H.Courtney, "Fundamental Structure-Property Relationships in Engineering Materials", in: ASM Handbook, Vol. 20: Materials Selection and Design, ASM International, pp. 336-356, 1997.

[33] C.Badini, "SiC Whiskers-Aluminum 6061 Composite: Microstructure and Mechanical Characteristics Anisotropy", J. Mat. Sci., Vol. 25, pp. 2607-2614, 1990.